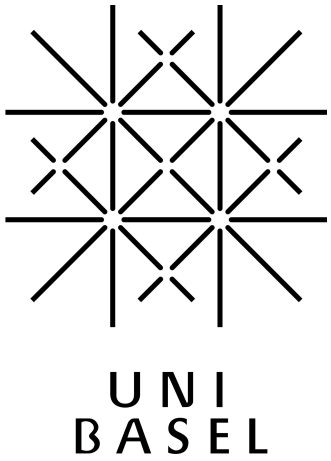

Biological Characterization of Functionalized Black Phosphorus Nanosheets

Thesis for the Master of Science in Nanoscience

Written by: Natalie Wichmann
Submitted to: Prof. Dr. Michael Nash
Research Group: Prof. Dr. Rainer Haag
Supervision: Prof. Dr. Mohsen Adeli, Dr. Katharina Achazi, Dr. Ievgen Donskyi
Date: February 28, 2020

Abstract

Since its discovery in 2014, Black Phosphorus (BP) nanosheets have emerged to be a promising platform for a broad range of applications such as electronics and optoelectronics, catalysis, energy storage and conversion as well as biomedicine. However, one major challenge of BP sheets is their low stability under ambient conditions which hampers their future applications. One of the most efficient methods to improve the stability of BP sheets is passivation of their surface by functionalization. Herein, the exfoliation of BP nanosheets, as well as their functionalization by ring-opening polymerization method is described followed by the analysis of the suitability for photothermal therapy. To prepare BP nanosheets, liquid phase exfoliation was performed in the polar aprotic solvents N-methyl-2-pyrrolidone (NMP) and 1,3-Dimethyl-3,4,5,6-tetrahydro-2(1H)-pyrimidinone (DMPU) which are both potent solvents, able to stabilize the exfoliated BP nanosheets. The obtained BP sheets were functionalized using a one-pot ring-opening co-polymerization of L-lactide and glycidol with two different molar ratios of monomers (Lactide:glycidol 1:1 and 1:2). While polyglycerol (PG) is water-soluble but non-biodegradable, L-lactide was used to introduce ester bonds that can be cleaved enzymatically. Polymerization of monomers on BP was performed in the solvents NMP and DMPU but the yield of the reaction in NMP was higher. The functionalized product exhibited a good water-solubility and an efficient photothermal effect. Cell viability assays showed a significantly reduced toxicity of the functionalized BP nanosheets compared to pristine BP sheets. The BP nanosheets show a superior drug loading efficiency even after functionalization caused by their negative surface charge thus being suitable for biomedical applications. The equimolar monomeric ratio of L-lactide to glycidol resulted in a significantly higher drug loading capacity and a more efficient photothermal effect of the functionalized BP nanosheets.

Contents

List of tables 1

List of figures 2

List of abbreviations 3

Introduction 4

Two-dimensional (2D) nanomaterials . . . 4

Graphene . . . 4

Further examples for 2D nanomaterials . . . 5

Black Phosphorus . . . 5

Exfoliation of Black Phosphorus nanosheets . . . 6

Stability under ambient conditions . . . 7

Functionalization of BP . . . 7

BP for biomedical applications . . . 8

Project objective 10

Experimental Section 12

Methods . . . 12

FTIR spectroscopy . . . 12

Dynamic light scattering (DLS) . . . 12

TEM . . . 12

Raman spectroscopy . . . 12

Thermogravimetric analysis (TGA) . . . 13

UV-Vis spectroscopy . . . 13

AFM . . . 13

Nuclear magnetic resonance (NMR) spectroscopy . . . 13

Microplate reader . . . 13

Fluorescence Microscopy . . . 13

Doxorubicin loading . . . 13

Photothermal Analysis . . . 14

CCK8 cell viability assay . . . 14

Live-dead cell viability assay . . . 14

Antimicrobial test . . . 15

Synthesis part . . . 16

Liquid Phase Exfoliation of Black Phosphorus . . . 16

Two-step Co-Polymerization: Synthesis of BP-PLA-PG (1:1) . . . 16

One-step Co-Polymerization . . . 16

Two-step Co-Polymerization: Synthesis of BP-PLA-PG (1:2) 17

Results and discussion **18**
Exfoliation of BP in NMP and DMPU 18
Functionalization of BP using a co-polymerization of L-lactide and glycidol . . . 23
In-vitro assays for biomedical applications 30

Conclusion and outlook **35**

Acknowledgements **36**

References **38**

Appendix - Supplementary data **42**

List of tables

Table 1 - Raman spectroscopy 22
Table 2 - Surface Zeta Potential 25
Table 3 - Doxorubicin loading capacity 31

List of figures

Fig. 1 - Black Phosphorus 5
Fig. 2 - Liquid phase exfoliation of BP 10
Fig. 3 - Reaction scheme 11
Fig. 4 - Exfoliation of BP 18
Fig. 5 - FTIR of exfoliated BP 19
Fig. 6 - TEM images of exfoliated BP 20
Fig. 7 - AFM of exfoliated BP 21
Fig. 8 - Raman spectroscopy of exfoliated BP 22
Fig. 9 - Functionalization of BP 23
Fig. 10 - FTIR spectra of sediments after functionalization 24
Fig. 11 - BP-PLA-PG (1:1) and (1:2) 25
Fig. 12 - FTIR of BP-PLA-PG (1:1) and (1:2) 26
Fig. 13 - TEM of BP-PLA-PG (1:1) and (1:2) 27
Fig. 14 - AFM of BP-PLA-PG (1:1) 28
Fig. 15 - TGA of BP-PLA-PG (1:1) and (1:2) 29
Fig. 16 - Photothermal effect 30
Fig. 17 - Drug loading calibration 31
Fig. 18 - Cell viability assay 32
Fig. 19 - Fluorescence images of the live-dead staining 33
Fig. 20 - Antimicrobial assay 34
Fig. 21 - ^{1}H NMR of BP-PLA-PG (1:1) and BP-PLA-PG (1:2) 43

List of abbreviations

BP - Black Phosphorus
NMP - N-methyl-2-pyrrolidone
DMPU - 1,3-Dimethyl-3,4,5,6-tetrahydro-2(1H)-pyrimidinone
PG - Polyglycerol
2D - Two-dimensional
h-BN - hexagonal boron nitride
TMD - Transition metal dichalcogenides
TMO - Transition metal oxides
CVD - Chemical vapour deposition
UV - Ultraviolet
IR - Infrared
NIR - Near infrared
DMSO - Dimethyl sulfoxide
DMF - Dimethyl formamide
hPG - Hyperbranched polyglycerol
PLA - Polylactide
FTIR - Fourier transform infrared spectroscopy
AFM - Atomic force microscopy
TEM - Transmission electron microscopy
$Sn(Oct)_2$ - Tin(II) 2-ethylhexanoate
BP-PLA - Black Phosphorus polylactide
BP-PLA-PG - Black Phosphorus polylactide polyglycerol
RPMI - Rosewell Park Memorial Institute
FBS - Fetal bovine serum
PBS - Phosphate buffered saline
CCK8 - Cell Counting Kit 8
DLS - Dynamic light scattering
TGA - Thermogravimetric analysis
NMR - Nuclear magnetic resonance
E. Coli - Escherichia Coli
OD - Optical density
CFU - Colony-forming units

Introduction

The field of nanoscience that started to emerge in the 1970s has gained tremendous scientific interest during the last decade and is evolving rapidly. Due to their drastically changed properties compared to their larger-scale analogues, nano-scale materials exhibit unique and fascinating behaviour and are therefore of huge scientific interest.[1] Nanomaterials can adapt various shapes and forms, making their applications plenty. The present report reflects on the study of phosphorene, a two-dimensional nanomaterial, that has gained tremendous scientific interest over the last decade.[2]

Two-dimensional (2D) nanomaterials

Nanomaterials can occur in zero-, one-, two- or three-dimensional crystal configurations and show a tremendously changed behaviour dependent on their structure. While most of these configurations are well studied, not much research has been spent on 2D materials.[2][3] These materials have a thickness of one to a few atoms and can either be layered or non-layered.[4] While layered nanomaterials show weak Van-der-Waals forces between the layers, in-plane bonds are strong.[3] Due to the high surface-area-to-volume ratio and the high number of atoms at the surface of the structure, 2D nanomaterials exhibit unique properties that are drastically changed compared to their bulk state.[3][5]

Graphene

Since the discovery of graphene in 2004, the flat monolayer of carbon atoms has gained tremendous scientific interest over the past decades. Graphene is an atomic layer of sp^2 hybridised carbon atoms that form a honeycomb lattice.[6] The residual electrons in the *p* bond are delocalised and form a π bond.[6] As 2D crystals were assumed to be thermodynamically highly unstable, the delamination of graphene from naturally abundant graphite opened up a whole new class of materials.[7] Due to the unique properties of graphene such as a high carrier mobility (10 000 $cm^2\ V^{-1}\ s^{-1}$),[2] high thermal and electrical conductivity (above 3 000 $W\ mK^{-1}$)[8] and a superior mechanical stiffness strength and elasticity.[6][8] Most commonly used methods to obtain graphene include mechanical exfoliation with the help of a scotch tape which results in high-quality graphene at low yields. By using solution-phase preparation methods, a high yield of graphene and graphene-derivatives can be obtained. However, the quality of the material is impaired. Chemical vapour deposition is a bottom-up method where graphene sheets are grown on a substrate by using methane as precursor. This method results in high-quality graphene at low yields.[6] The applications of graphene are highly versatile due to the unique properties of the material and include electronics and optoelectronics,

catalysis, energy storage and conversion, as well as biomedical applications.[2] Due to the large surface area, graphene has a superior drug loading capacity and a high photothermal efficiency, that makes it a promising platform for theranostics. However, one limiting factor for graphene when it comes to *in vivo* studies is its accumulation in the body and its cytotoxicity.[9][10]

Further examples for 2D nanomaterials

Even though graphene was the first 2D nanomaterial to be discovered and is the most famous one yet, much research has been spent on the discovery of other materials exhibiting similarly unique electrochemical and physical properties.[5] Further examples are hexagonal boron nitride (h-BN),[11] transition metal dichalcogenides (TMDs), such as MoS_2, TiS_2, TaS_2, WS_2, $MoSe_2$ or WSe_2, transition metal oxides (TMOs),[12][13] silicene,[14] germanene,[13] phosphorene[12] or borophene.[15] All these materials exhibit drastically changed properties compared to their bulk state.[1] A number of synthetic strategies has been developed to produce ultrathin nanomaterials. These include mechanical cleavage, liquid phase exfoliation, ion-intercalation exfoliation, selective etching exfoliation, chemical vapor deposition (CVD) and wet-chemical synthesis.[2] A lot of research has already been spent on the thorough characterization of these mostly novel materials. The present report reflects on the functionalization and characterization of BP as a 2D nanomaterial.

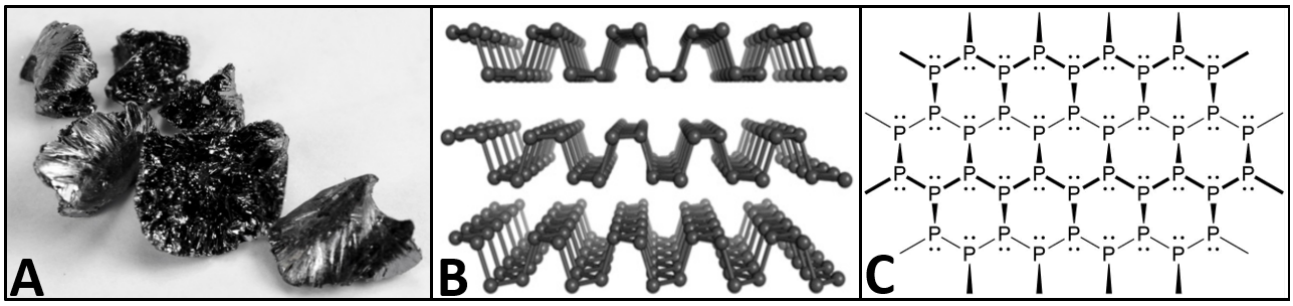

Figure 1 – Black Phosphorus. **A:** Bulk BP.[16] **B:** Side view of monolayers in BP, held together by Van-der-Waals forces.[17] **C:** Scheme of top view of phosphorene.

Beside graphene, phosphorene (2D BP) was the first synthesized 2D elemental allotrope to be discovered and has gained much scientific interest ever since, especially for nanoelectronics and nanophotonics.[18][19] Due to its tunable bandgap of almost 2 eV, which bridges the range between the bandgap of graphene and TMDs, phosphorene appeared to be a potent material with versatile applications.[18][20][21] As its degradation under physiological conditions results in materials of low toxicity, it can not only be used for optoelectronic purposes, but also theranostics and biomedicine.[1][10][20] However, one factor impeding the versatility of phosphorene is its low stability under ambient conditions as well as its challenging synthesis.[22]

Black Phosphorus

First reports of BP started to emerge one century ago, when Bridgman *et al.* obtained BP from the conversion of White Phosphorus by applying high pressure (1.2 GPa) and temperature (200 °C) to the crystal.[23] However, BP did not receive much attention until 2014, when Li *et al.* successfully exfoliated BP sheets that were several nanometers in thickness (so-called nanosheets).[10] Bulk BP is a crystalline material that consists of distinct atomic layers which are held together by weak Van-der-Waals interactions. Each Phosphorus atom is covalently bonded to three adjacent Phosphorus atoms which results in a non-planar honeycomb lattice structure.[10] Opposed to graphene, BP is a direct bandgap semiconductor with a thickness-dependent bandgap. While bulk BP has a bandgap of 0.3 eV, decreased interlayer interactions cause the bandgap to increase for monolayer BP which has a bandgap of 2 eV.[10][18] This tunable bandgap enables the absorption of light across the ultraviolet (UV) and infrared (IR) regions.[24][25] Furthermore, BP nanosheets exhibit good conductivity and high electron mobility making the material interesting for a variety of applications such as transistors, photovoltaic devices, sensing and photodetectors.[5] Due to the large abundance of Phosphorus in the human body (approx. 1 % of the human body mass), BP appears to be a very convenient biocompatible material to be used for biomedical applications.[21] The degradation under ambient conditions to phosphonates and phosphates is one major advantage of BP compared to other two-dimensional nanomaterials.[1][24] Another feature which makes phosphorene an interesting material for theranostics is its good photothermal property. Especially ultrasmall BP sheets exhibit a large near-infrared (NIR) extinction coefficient[24] that is highly efficient for photothermal therapy.[20]

Exfoliation of Black Phosphorus nanosheets

To be able to use phosphorene for any applications, it is necessary to produce high-quality BP nanosheets at a large scale. Due to the increased interlayer cohesion in bulk BP compared to graphene, which arises from the free lone electron pair on each Phosphorus atom, the delamination of monolayers is slightly more challenging than it is for graphene.[26] However, there are several successful approaches for the exfoliation of BP nanosheets. Mechanical cleavage using a sticky tape was the first reported method for the exfoliation of BP.[10] Even though this method resulted in BP nanosheets of a few nanometers in thickness, the yield was very low and the delaminated sheets needed to be stabilized by a substrate. Thus, the method was inconvenient for the exfoliation of BP sheets at a larger scale.[2] The method of choice for the exfoliation of BP at large scale is the liquid phase exfoliation, where bulk BP is ultrasonicated in an organic solvent to exfoliate the distinct nanosheets. Commonly, NMP is used as solvent for the

exfoliation, as it balances the surface energy of BP.[27] However, it is difficult to be removed from the exfoliated BP nanosheets which is the reason why many other organic solvents such as dimethyl sulfoxide (DMSO), dimethylformamide (DMF) or formamide have been used successfully for the exfoliation of BP.[28] Sun *et al.* (2018) claimed that DMPU is an even more potent solvent for the exfoliation of BP nanosheets.[26] Thus, liquid phase exfoliation is a very efficient, scalable and commonly used process for the preparation of BP nanosheets. The present report reflects on the liquid phase exfoliation using the organic polar aprotic solvents NMP and DMPU.

Stability under ambient conditions

One major drawback that is limiting the applications of BP is its low stability under ambient conditions. The free lone electron pair on each Phosphorus atom can easily react with water or oxygen, causing the degradation of the material to phosphate and phosphonates.[24][29] Furthermore, the large surface area of BP nanosheets contributes to the high reactivity with oxygen and water. The degradation can also be induced by light and occurs within several days of exposure.[30] Thorough degradation studies have been conducted that could show how bubble formation is one major sign of degradation.[31] The oxidation of pristine BP nanosheets of several nanometers in height can be observed using Raman spectroscopy. Pristine BP exhibits three distinct peaks in Raman spectroscopy correlating to the A^1_g (361 cm^{-1}), B_{2g} (438 cm^{-1}) and A^2_g (466 cm^{-1}) vibrational modes of the nanosheets.[30] The integrated peak ratio A^1_g / A^2_g indicates the level of degradation as values lower than 0.2 correspond to high levels of oxidation on the sheets.[30] The high reactivity of BP with oxygen or water and the resulting degradation of the sheets are the major reasons why the establishment of the material for any kind of application is highly challenging. The stability of BP sheets could be improved by several approaches. By inorganic coatings, the BP surface can be shielded from oxygen and thus it prevents the degradation of the material. Suited coatings that were proven to enhance the surface stability are for example Aluminium oxide[32] and Boron nitride.[33] By passivating the lone electron pairs of phosphorene, the surface stability can be significantly increased.[34] Another approach aims to passivate the surface by covalent functionalization and thus keeping the lone electron pairs covalently paired. The passivation of the surface was successfully shown using aryl diazonium functionalization[35] as well as other nucleophilic additions that led to P-C and P-O-C bonds.[22] Furthermore, using azide passivation, the BP surface can be successfully passivated by P=N double bonds.[22] Herein, the surface is aimed to be functionalized with a copolymer to achieve a good water-solubility and low-rate biodegradability.

Functionalization of BP

Since BP is only dispersible but not dissolvable in water which is necessary for biomedical applications under physiological conditions, polyglycerol is a suitable candidate for the functionalization of BP. Hyperbranched polyglycerol (hPG) exhibits high biocompatibility, functionality and thermal stability as well as a low toxicity[36][37][38][39] which are crucial factors for biomedical applications and one reason why hPG has gained tremendous scientific interest in biomedical research. Furthermore, hPG exhibits low immunogenicity as well as a long blood circulation time which is dependent on the molecular weight of the polymer.[39][40] The synthesis of hPG can be performed via a cationic or anionic ring-opening polymerization starting from glycidol.[36] The properties of hPG are highly dependent on the functionality and the molecular weight. Due to the hyperbranching, hPG has a three-dimensional structure with many endgroups that can be tuned easily.[38] One major drawback of hPG for biomedical applications is the fact that it is non-biodegradable. While hPG of low molecular weight is secreted through renal clearance,[38] high molecular weight hPG is found to accumulate in the liver and spleen.[41] Different strategies are aiming to circumvent the non-biodegradability of hPG. One approach to increase the degradability of the hPG backbone is to introduce bonds that are degradable under acidic conditions (pH 5). Even though that increases the degradability of hPGs, the stability under neutral conditions is deteriorated.[40] Another approach exploits the fact that esterase enzymes and acidic conditions are present in living cells. Therefore, the introduction of ester bonds in the PG network can increase the degradability under physiological conditions.[40] One highly convenient biodegradable polymer is polylactide (PLA) that is suited for biomedical applications due to its high biocompatibility and loading capacity towards therapeutic agents.[42] The degradation of PLA in aqueous solution occurs via hydrolysis which takes several months.[43][44][45] However, due to the abundance of hydrolases in living cells, the degradability in physiological conditions is enhanced.[46][47] PLA can be obtained from the direct condensation of lactic acid which is a naturally occurring organic acid or in a catalysed ring-opening polymerization using cyclic lactide. However, due to the low functionality and its water-insolubility, PLA on its own is not convenient for biomedical applications. Therefore, it is often used being co-polymerized with other suitable polymers such as PG.[44] Blended with PG, PLA co-polymers can be water-soluble and biocompatible, as well as biodegradable which is optimal for biomedical applications.[42][44]

BP for biomedical applications

Compared to other 2D nanomaterials, BP exhibits a range of properties which make it a promising platform for theranostics and biomedicine.[48] However, the high reactivity

of BP with oxygen and air is the main reason why the potential of BP for biomedicine has not been fully exploited yet. Since many strategies have been determined that successfully passivate the surface of BP nanosheets, research on the potential biomedical applications of BP gained much more interest.[1][22][48] Due to its tunable and direct bandgap, BP shows excellent optical properties that could be used for fluorescent and colorimetric studies of biological compounds such as proteins or nucleic acids.[48] The absorption of light from IR to UV regions makes BP a suitable candidate for applications such as bioimaging, biosensing, photoacoustic imaging, photodynamic and photothermal therapy or drug delivery.[25][48][49] One major advantage of BP compared to all other 2D nanomaterials discovered to date is the large abundance of Phosphorus in living cells. As DNA, which forms the base of all living organisms, contains a high amount of Phosphorus, BP appears to be highly convenient to be used for biomedical applications.[49]

Photothermal effect

Photothermal therapy is a promising concept for the treatment of cancer with minimal invasiveness. NIR laser light can penetrate tissue without damaging it and by using a photothermal agent, the optical energy is converted into thermal energy.[50] A suited photothermal agent is required to have an efficient photothermal conversion and a large extinction coefficient in the NIR region. Furthermore, high biocompatibility and biodegradability are necessary properties of a photothermal agent in order to prevent accumulation.[49][51] These requirements are met by BP which has been shown in previous studies and therefore, BP is a promising material for future theranostics.[49][51]

Drug loading capacity

Carriers that can distribute therapeutic agents to their destination are of great importance in modern medicine. Due to the large surface area and the highly negative charge on the surface caused by the presence of phosphoric acid, BP is able to absorb a huge amount of suited cationic therapeutic agents such as doxorubicin, vinorelbine or topotecan.[49][52] Combined with photothermal therapy, the drug release could even be induced by irradiation with NIR laser light.[49][53]

Further potential applications of BP in biomedicine include photodynamic therapy,[54] tissue engineering and 3D printing,[49] as well as diagnostic applications such as fluorescence and photothermal imaging.[49][51]

Project objective

The first step of the project was supposed to be the exfoliation of BP nanosheets. This part aimed to address questions such as what are the best conditions for the exfoliation of BP and are both solvents NMP and DMPU as suitable for the exfoliation of BP as claimed in previous publications? Therefore, in a comparative study, liquid phase exfoliation was performed in NMP and DMPU. Liquid phase exfoliation was based on the ultrasonication of bulk BP in a solvent (fig. 2). The exfoliated BP nanosheets were characterized by Fourier Transform IR (FTIR) and Raman spectroscopy, atomic force microscopy (AFM), as well as transmission electron microscopy (TEM) in order to compare the quality of the exfoliated BP nanosheets.

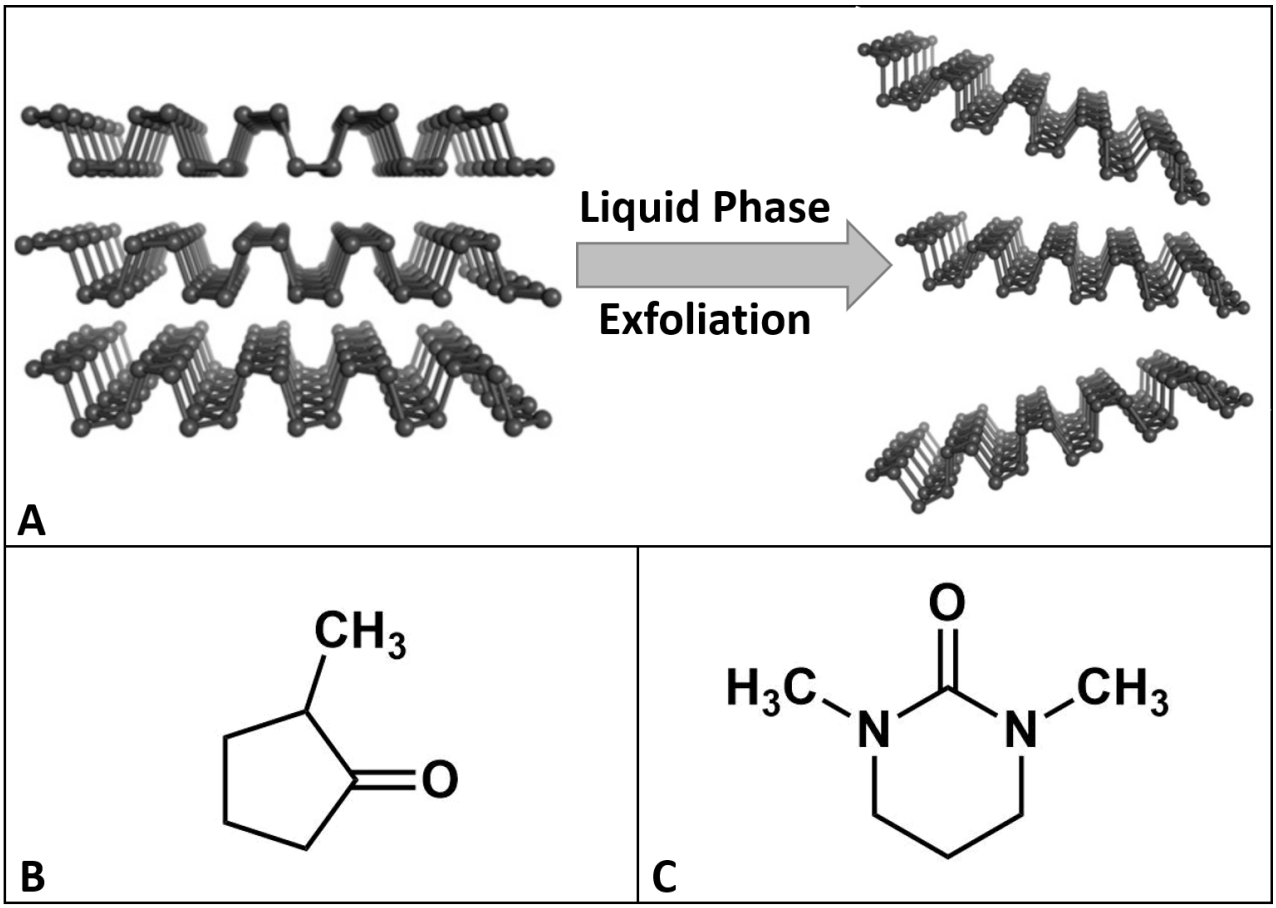

Figure 2 – Liquid phase exfoliation of BP. **A:** Scheme of the liquid phase exfoliation using an ultrasonication bath.[17] **B & C:** Chemical formula of the used solvents for liquid phase exfoliation NMP and DMPU.

The second part of the project was aiming at the functionalization of the exfoliated BP nanosheets. Whether BP is a sufficient nucleophile to start the polymerization of glycidol and lactide and whether the functionalization could enhance the stability of the BP nanosheets were questions ought to be addressed by this part of the project.

Two different approaches were envisioned. The first ought to yield BP nanosheets that are coated with PLA first and PG on top of the PLA layer. In that reaction, it was expected to achieve water-soluble and biodegradable, as well as biocompatible BP nanosheets (fig. 3 A). A second approach that was supposed to be tested was a one-step co-polymerization, where both monomers lactide and glycidol ought to be co-polymerized to the BP surface randomly (fig. 3 B). Both reactions were conducted in NMP and DMPU in parallel to determine whether either solvent is better suited for the functionalization. The reaction parameters were set to be consistent during all reactions with a reaction temperature of 120 °C for 24 hours with same amounts of Tin(II) 2-ethylhexanoate ($Sn(Oct)_2$) as catalyst.

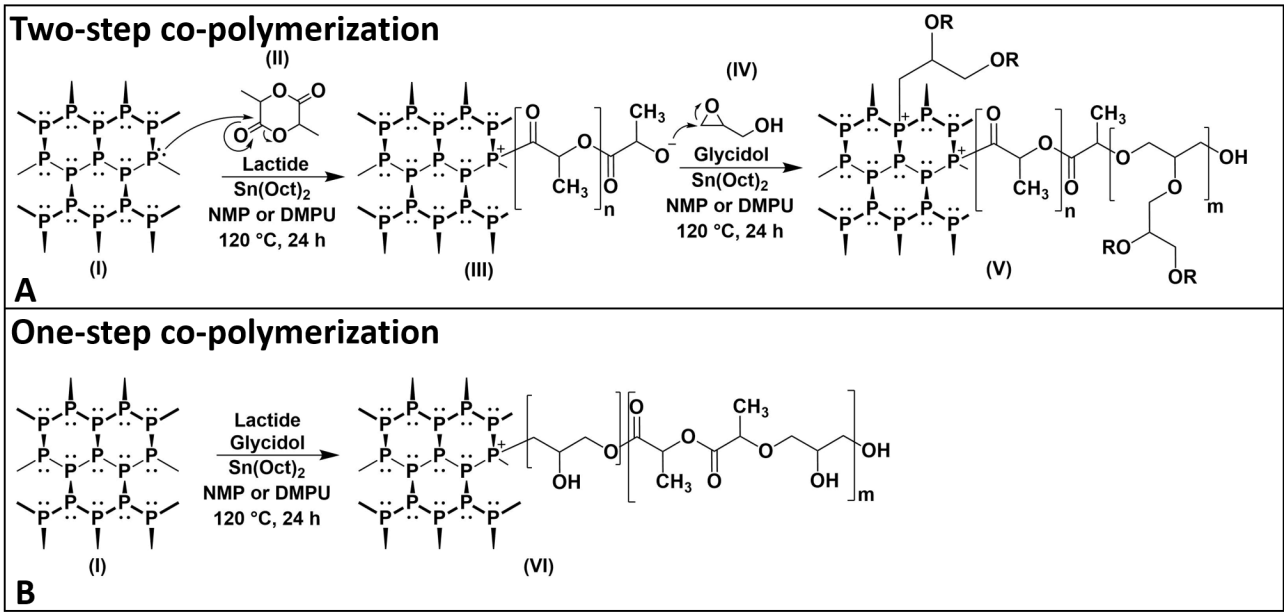

Figure 3 – Reaction scheme. **A:** Mechanism for the step-wise co-polymerization of BP nanosheets. In the first reaction step, lactide (II) was added to the exfoliated BP (I). To the reaction mixture (containing BP-PLA (III)), glycidol (IV) was added to obtain the final product BP-PLA-PG (V). **B:** Scheme of the one-pot co-polymerization reaction. Addition of both monomers occurred at the same time to obtain the product (VI) which ought to have a random order of polymer segments. Bonds without atom indicate the continuous BP sheets that are schematically drawn.

The last step of the project aimed to test whether the functionalized BP sheets would show a good loading capacity for therapeutic agents and whether the functionalization changes the properties and the toxicity compared to pristine BP. Therefore, the cell viability after incubating HeLa cells as well as bacterial cells with the synthesized samples was analysed. Furthermore, the photothermal effect of the samples ought to be analysed to test whether photothermal therapy would be a promising application for the samples.

Experimental Section

Methods

All experiments were conducted at the Department of Biology, Chemistry, Pharmacy of the Freie Universität Berlin. All chemicals and organic solvents were of analytical grade and obtained from commercial sources unless stated otherwise. Bulk BP was purchased from smart elements. DMPU, NMP, L-lactide, glycidol and $Sn(Oct)_2$ were purchased from Sigma-Aldrich. Doxorubicin hydrochloride was purchased from abcr GmbH. The purification was performed using dialysis tubes (50 kDa MWCO) purchased from Sigma-Aldrich.
All biological experiments were performed according to the German Genetic Engineering Law and German Biosafety Guidelines in Laboratory, Level 1. Rosewell Park Memorial Institute (RPMI) medium was purchased from Gibco. Fetal bovine serum (FBS), Dulbecco's phosphate-buffered saline (PBS), penicillin-streptomycin, Cell Counting Kit 8 (CCK8) solution and Trypsin-EDTA solution were purchased from Sigma-Aldrich. HeLa cells were obtained from the DSMZ.

FTIR spectroscopy

IR spectroscopy was performed using an FT/IR-4100 (Jasco) with a TGS detector from 4000 to 650 cm^{-1}. Samples were measured at room temperature in solid form by adding small amounts of the sample to the crystal.

Dynamic light scattering (DLS)

DLS and zeta potential measurements were performed in ultrapure water at room temperature on a Zetasizer Ultra (Malvern Panalytical).

TEM

TEM images were obtained using a Talos L120C TEM (Thermo Fisher Scientific). Non-functionalized samples were drop-casted being dispersed in ethanol, while functionalized samples were drop-casted being dissolved in water. All samples were analyzed under ambient conditions at room temperature.

Raman spectroscopy

Raman spectroscopy was performed using a Horiba Xplora spectrometer equipped with a 532 nm laser and 10x and 100x objectives. All samples were drop-casted onto silicon wafers. For the non-functionalized samples, the wafers were ultrasonicated for

10 minutes in acetone before adding the sample in either NMP or DMPU. The prepared wafers were dried and kept under vacuum until being used to avoid degradation. For functionalized samples, the wafers were drowned in piranha solution (sulfuric acid : 30 % hydrogen peroxide solution 3:1) before drop-casting the aqueous solution. The wafers were dried on a heating plate at 50 °C for at least one hour.

Thermogravimetric analysis (TGA)

For all TGA experiments, a LINSEIS STA PT1600 (TG – DTA/DSC) device was used. The experiments were performed in air with a heating rate set to 10 °C min^{-1}. Calibration curves were obtained for each sample and the measurements were performed in Al_2O_3 crucibles. The used sample mass varied from 10 to 25 mg.

UV-Vis spectroscopy

UV-Vis spectroscopy was performed using an Agilent Cary 8454 UV-Visible spectrophotometer. Samples were measured in ultrapure water at room temperature.

AFM

AFM images were recorded using a MultiMode Nanoscope V scanning probe microscopy (SPM) system (Bruker, USA) in air under ambient conditions. Commercially available AFM cantilever tips with a force constant of 48 N/m and a resonance frequency of 330 kHz were used. The images were obtained in peak force mode and the scanning rate was set to 0.8 Hz.

Nuclear magnetic resonance (NMR) spectroscopy

Proton NMR was recorded using an ECZ600 S NMR spectrometer (JEOL) using a resonace frequency of 600 MHz.

Microplate reader

For the cell viability assay, the absorption of the CCK8 solution was determined using a TECAN infinite M200 Pro microplate reader at a wavelength of 450 nm and a reference wavelength of 600 nm.

Fluorescence Microscopy

For the fluorescence microscopy, a Zeiss Axiovert 200 microscope, equipped with 10x and 100x objective, Hxp 120 c lightning unit and an AxioCam MRm camera was used.

Doxorubicin loading

A calibration curve relating the doxorubicin concentrations to the UV-Vis absorption was obtained by measuring the absorption of doxorubicin dissolved in water for five different concentrations. Exfoliated BP (2 mg) was dispersed in water (1 mL) and Doxorubicin hydrochloride (4 mg) was added. The mixture was vigorously stirred at room temperature overnight. Subsequently, the mixture was transferred to a centrifugation tube and centrifuged for 10 minutes at 10 000 rpm (36 894 x *g*). The supernatant was collected and diluted until it was in the range of the calibration curve. The drug loading was calculated by subtracting the amount of doxorubicin in the supernatant from the initial concentration. The functionalized samples (3 mg) were both dissolved in water (1 mL) and doxorubicin hydrochloride (6 mg) was added. The mixtures were stirred overnight. Subsequently, methanol (100 µL) and cold acetone (25 mL) were added causing white precipitation. The mixtures were centrifuged for 10 minutes at 10 000 rpm (36 894 x *g*) and the sediment was redissolved in water (1 mL). The doxorubicin concentration was determined by measuring the absorption.

Photothermal Analysis

To determine the photothermal efficiency of the functionalized samples, BP-PLA-PG (1:1) and BP-PLA-PG (1:2) were dissolved in water to final concentrations of 3 mg/mL. Non-functionalized BP (2 mg) was dispersed in water (1 mL). Subsequently, 50 µL of each sample was placed in an Eppendorf tube (0.5 mL). For the irradiation, an FC-D-785 laser module was used at a wavelength of 785 nm. To detect the temperature, an infrared thermal imaging camera (FLIR E30) was used. The temperature was measured every 10 seconds for at least 4 minutes.

CCK8 cell viability assay

HeLa cells were cultured in RPMI 1640 medium (Gibco) supplemented with 10 % (v/v) FBS and 1 % (v/v) penicillin / streptomycin. The cells were incubated under humidified conditions under 5 % CO_2 at 37 °C. 24 hours before the test, the cells ($5 \cdot 10^4$ cells/mL) were seeded in a 96-well plate and incubated. Non-functionalized and functionalized BP samples dissolved in water (10 mg/mL) were added to the medium-covered wells such that final concentrations between 1 mg/mL and 0.001 mg/mL were reached and incubated for 24 hours. Each concentration of each sample was measured in duplicates. Subsequently, CCK8 solution (10 µL) was added to each well and after an incubation time of three hours, the absorption of the wells at 450 nm was measured using a microplate reader. Cells without treatment and cells treated with SDS (10 %) were used as negative and positive controls. The test was repeated three times.

Live-dead cell viability assay

For the live-dead staining, a live dead viability cytotoxicity kit (Invitrogen) was used. HeLa cells were cultured in RPMI 1640 medium (Gibco) supplemented with 10 % (v/v) FBS and 1 % (v/v) penicillin / streptomycin. The cells were incubated under humidified conditions under 5 % CO_2 at 37 °C. 24 hours before the test, the cells ($5 \cdot 10^4$ cells/mL) were seeded in a 96-well plate and incubated. Non-functionalized and functionalized BP samples dissolved in water (10 mg/mL) were added to the medium-covered wells such that final concentrations between 1 mg/mL and 0.001 mg/mL were reached and incubated for 24 hours. After that, the medium was removed and the cells were washed with PBS twice. A solution of ethidium homodimer (2 mM in DMSO / H_2O 1:4 (v/v), 6 µL) in PBS (3 mL) was prepared and vortexed well. To that solution, calcein acetoxymethyl ester (4 mM in anhydrous DMSO, 1.5 µL) was added and the solution was mixed well. To the medium-removed wells, the prepared staining solution (100 µL / well) was added and the plate was incubated for 30 minutes before being analysed using a fluorescence microscope. The test was repeated three times.

Antimicrobial test

For the antimicrobial test, Agar plates were prepared by dissolving LB-Agar (20 mg) in distilled water (500 mL) and autoclaving the solution. The solution was poured into Petri dishes and left to dry in a laminar flow hood. *Escherichia Coli* (E. Coli) ORN208 cells were cultured in LB medium at 37 °C overnight. Subsequently, the optical density (OD) was determined using a microplate reader and the suspension was diluted with low salt LB medium until an OD of 0.28 was reached. Thereafter, the suspension was diluted 10 000 fold until a concentration of 10^4 cells/mL was reached. The non-functionalized and the functionalized BP samples (0.2 mg/mL), as well as a water and SDS (10%) control, were mixed with the bacteria solution in a 1:1 volume ratio. To be able to determine the bacterial concentration at the beginning of the test, the suspension mixed with water was plated on the Agar plates in one- and ten-fold dilutions. All suspensions were incubated at 37 °C under constant shaking for 2 hours. Subsequently, they were plated on Agar plates in ten- and hundred-fold dilutions. After another 2 hours, the procedure was repeated with hundred- and thousand-fold dilutions of the bacterial suspensions. All plates were prepared in duplicates. After incubating the plates overnight at 37 °C, the colonies were counted.

Synthesis part

Liquid Phase Exfoliation of Black Phosphorus

Liquid phase exfoliation was performed in NMP and DMPU. For better comparison, both experiments were carried out at the same time. Therefore, bulk BP (100 mg) was added to two 50 mL round bottom flasks in a glove box. The flasks were sealed and removed from the argon atmosphere. To one of these flasks, NMP (20 mL) was added, while to the other flask DMPU (20 mL) was added. Both flasks were submerged in an ultrasonication bath filled with ice-cold water for 2 hours. After that, the dispersions were filled into centrifugation tubes (50 mL, Falcon) and centrifuged (30 min, 1 500 rpm (226 x *g*), 4 °C) to remove all unexfoliated BP. The supernatant was transferred to centrifugation tubes and centrifuged (45 min, 10 000 rpm (36 894 x *g*), 4 °C) three times while removing the supernatant and redispersing the exfoliated BP in water after each centrifugation. The product was obtained after lyophilization as black powder (Yield: NMP (39.8 mg), DMPU (35.7 mg)).

Two-step Co-Polymerization: Synthesis of BP-PLA-PG (1:1)

All polymerization reactions were carried out under inert conditions at the Schlenk line. The co-polymerization was performed in NMP and DMPU in parallel. Therefore, to two 100 mL round-bottom flasks equipped with stirring bars, exfoliated BP (10 mg) and L-lactide (500 mg, 3.47 mmol) were added. The flasks were evacuated and argon flushed three times. Subsequently, the respective solvent (20 mL) was added to the respective flask and catalytic amounts of $Sn(Oct)_2$ (0.01 mL) were added. The mixture was stirred at 120 °C for 24 hours. After that, distilled glycidol (0.23 mL, 3.47 mmol) was added dropwise, using a syringe pump. The reaction was stirred for another 24 hours at 120 °C. The reaction mixture was transferred to a 50 mL centrifugation tube and centrifuged at 36 894 x *g* for 30 minutes. The sediment was redispersed in DMF/Methanol (1:1) and centrifuged at the same conditions three times. Subsequently, the centrifugation was repeated at least three times by redispersing the sediment in water. The sediment dispersed in water was lyophilized and the product was obtained as black solid (NMP: 4.1 mg, DMPU: 1.7 mg). The supernatant of all centrifugation steps for the reaction in NMP was collected in a flask and dialysed for at least 4 days against water while changing the solvent three times per day (50 kDa MWCO). The aqueous solution was lyophilized and the product was obtained as brown solid (36.6 mg).

One-step Co-Polymerization

The co-polymerization of lactide and glycidol to exfoliated BP was performed in NMP and DMPU for comparison. Therefore, exfoliated BP (10 mg) and L-lactide (500 mg,

3.47 mmol) were added to two 100 mL round-bottom flasks equipped with stirring bars. Both flasks were evacuated and argon flushed. The respective solvent (20 mL) was added to the respective flask and $Sn(Oct)_2$ (0.01 mL) was added as catalyst. The reaction mixtures were heated up to 120 °C and distilled glycidol (0.23 mL, 3.47 mmol) was added drop-wise with the help of a syringe pump. Both reactions were stirred at 120 °C for 24 hours. After that, both reaction mixtures were centrifuged at 36 894 x *g* for 30 minutes and the sediment was redispersed in DMF/Methanol (1:1) three times. The centrifugation was repeated at least three times by redispersing the sediment in water. The aqueous solution was lyophilized and the product was obtained as black solid (NMP: 7.6 mg, DMPU: 7.2 mg).

Two-step Co-Polymerization: Synthesis of BP-PLA-PG (1:2)

The synthesis of BP-PLA-PG (1:1) was conducted in the same way as the synthesis of BP-PLA-PG (1:2), but instead of using equimolar ratios of monomers, the amount of used distilled glycidol was doubled. The reaction was performed in NMP and all other steps were conducted as described above.

Results and discussion

Exfoliation of BP in NMP and DMPU

The first aim of the project was the exfoliation of pristine BP nanosheets with lateral sizes up to 1 µm. To obtain a sufficient yield for further studies, liquid phase exfoliation was chosen to delaminate the sheets from the bulk crystal. For the liquid phase exfoliation, bulk BP was mildly ground and dissolved in a polar aprotic organic solvent. After ultrasonication for two hours, the dispersion was centrifuged in water several times and lyophilized. To compare the suitability of the solvents NMP and DMPU, two batches of BP were exfoliated in a comparative study. While bulk BP is a shiny black crystal (fig. 4 A), it can be ground quite easily yielding flat black crystal layers of several millimetres in height and up to one centimetre in lateral sizes (fig. 4 B). These ground crystals do not disperse in NMP or DMPU. However, after the first minutes of ultrasonication, BP starts to disperse in both solvents resulting in a deep brown colour of the dispersion. After liquid phase exfoliation, BP is very well dispersible in either solvent (fig. 4 C) with no visible difference observable. In terms of yield, both solvents showed comparable results; the exfoliation in NMP yielded 40 %, while the exfoliation in DMPU yielded 36 % after lyophilization (fig. 4 D).

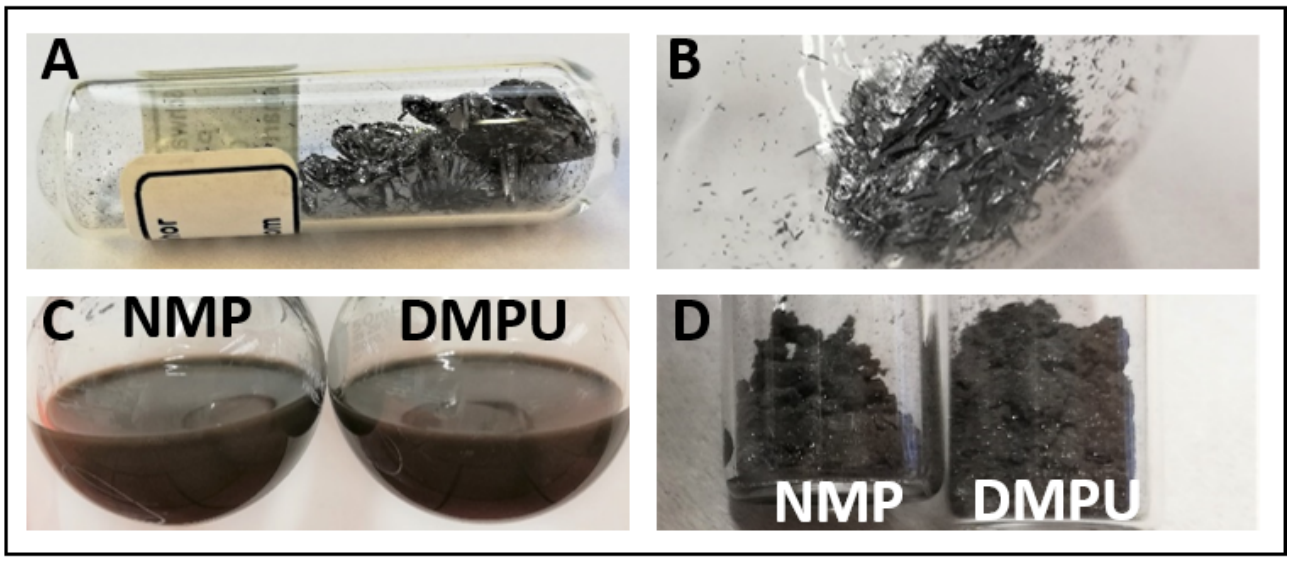

Figure 4 – Exfoliation of BP. **A:** Bulk BP in an argon-filled glass ampoule. **B:** Ground BP in an argon-filled flask. **C:** Exfoliated BP dispersed in the respective solvent. **D:** Dried exfoliated BP after lyophilization.

By comparing several batches of BP exfoliated in NMP, it could be observed that the yield is highly dependent on the previous grinding of the bulk BP. If the BP crystals were not ground sufficiently, the yield will be considerably lower. Furthermore, the density of the nanosheets exfoliated in NMP seems to be significantly higher (fig. 4 D). Another

important factor during the exfoliation of BP turned out to be the temperature during ultrasonication. Since the temperature constantly increased during ultrasonication, the temperature was controlled using an ice-bath.
As all the bonds in BP are symmetric and do not change their dipole moment, BP is FTIR inactive which is indicated by the absence of any peaks (fig. 5). Furthermore, FTIR analysis yields no difference for both exfoliation batches and clearly shows the absence of oxygen on the nanosheets. High amounts of oxygen would be indicated by a significant peak at 1000 cm $^{-1}$.[18][29][55]

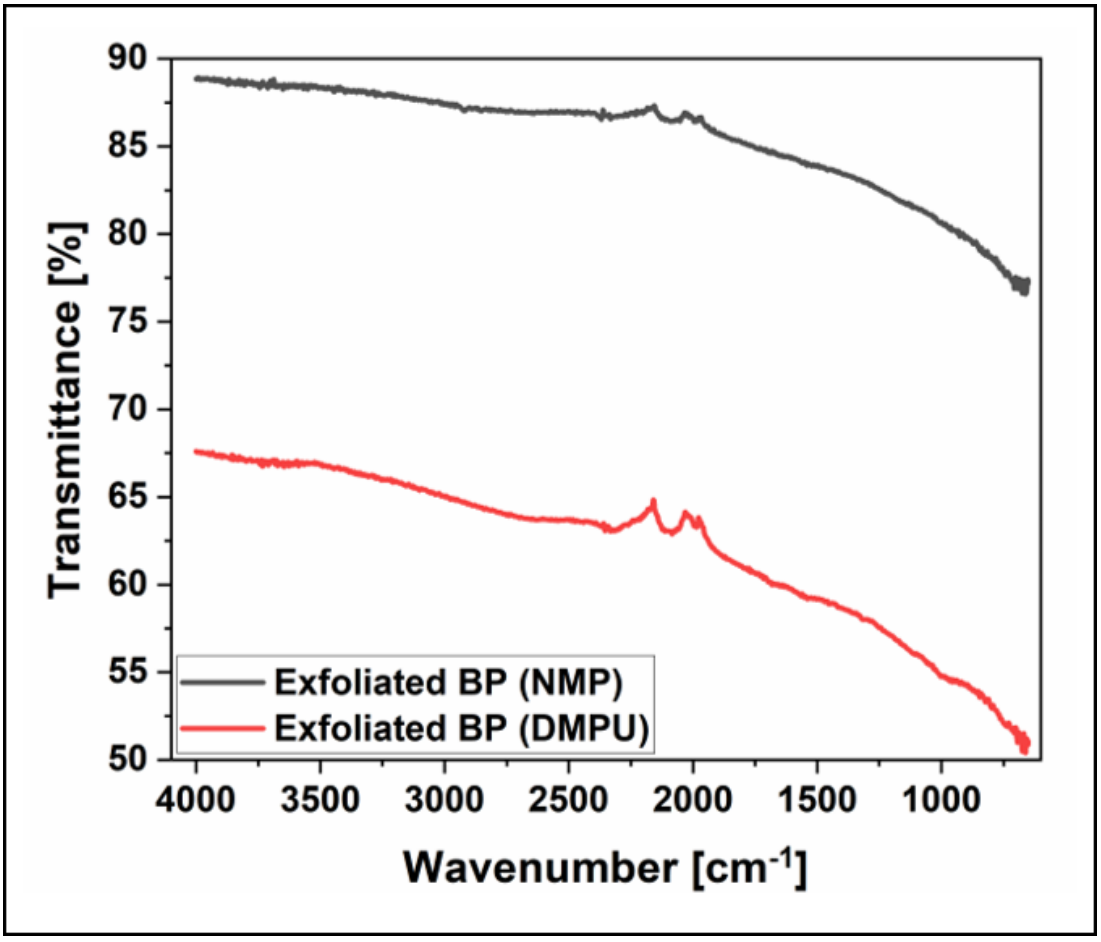

Figure 5 – FTIR of exfoliated BP. Black line: FTIR of BP exfoliated in NMP. Red line: FTIR of BP exfoliated in DMPU.

To obtain a better insight into the overall structure of the exfoliated BP, TEM analysis was performed on 9 nanosheets for each exfoliation batch. The obtained images (fig. 6) show that the lateral sizes for the exfoliated sheets range from 100 nm to 1 µm. Furthermore, the images show sharp edges of the sheets suggesting that the exfoliation did not yield monolayers but rather stacks of several sheets on top of each other. Possible reasons for the stacking of the sheets might be that either the exfoliation time of two hours was not sufficient to exfoliate monolayers or the sample preparation for the

TEM analysis was inconvenient. Since the exfoliated BP was kept in ethanol before being drop-casted on the carbon grid, the evaporation of the ethanol might have caused the sheets to restack and form aggregates. However, no obvious difference between the exfoliation of BP in NMP (fig. 6 A & B) or DMPU (fig. 6 C & D) could be observed. Furthermore, it is possible to conclude from these images that exfoliated BP is stable in ethanol as there are no signs of degradation. The obtained TEM images are comparable to previous studies on BP nanosheets.[25][29]

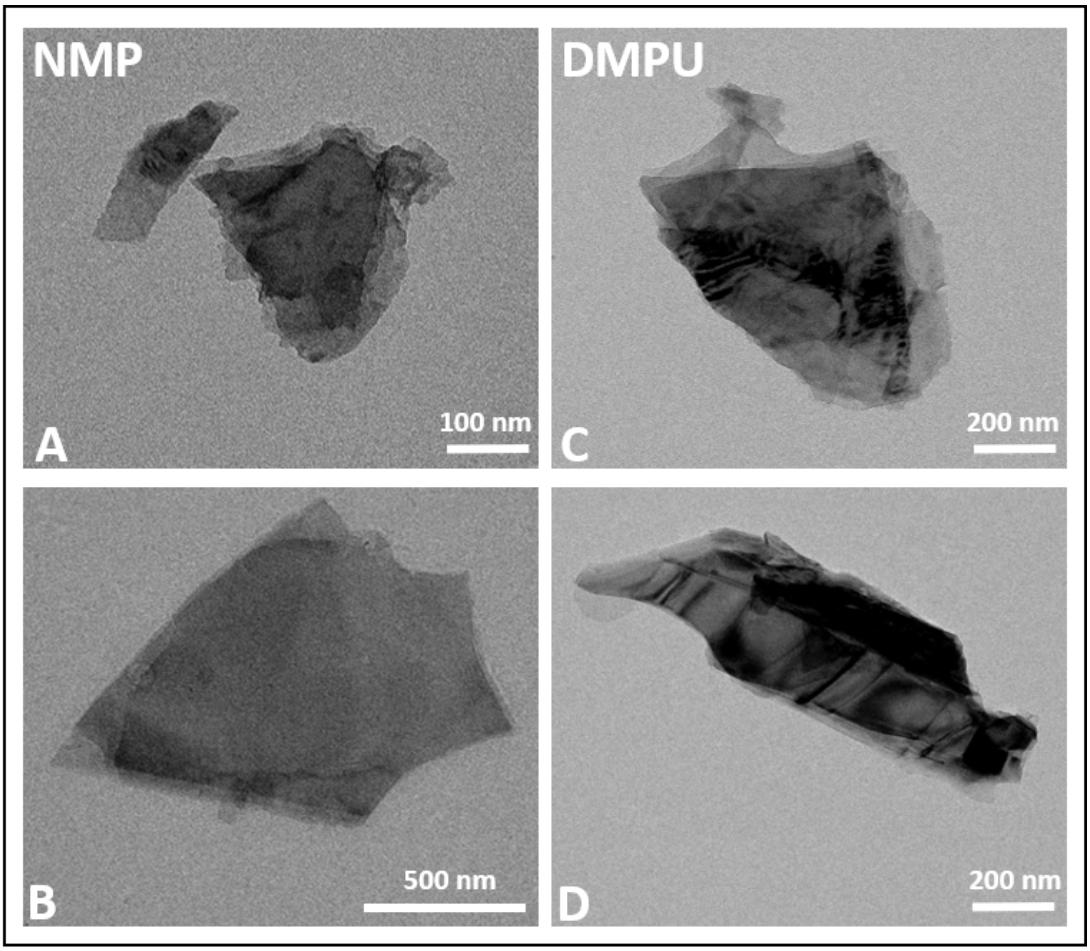

Figure 6 – TEM images of exfoliated BP. **A & B:**TEM images of BP exfoliated in NMP. **C & D:** TEM images of BP exfoliated in DMPU.

To obtain an insight into the height of the exfoliated nanosheets, AFM was performed (fig. 7). The lateral sizes suggested by AFM, which range from 300 nm to 1 µm, are slightly larger than the ones observed by TEM analysis. Furthermore, the images do not show a smooth surface which is confirmed by the height profile deducted from the AFM analysis (fig. 7 B). Since there are no plateaus present in the profile which would be expected from 2D materials, the rather high peaks might arise from aggregation and folding of the nanosheets. One possible explanation might be again the sample preparation, as the BP sample was dispersed in ethanol before being drop-casted onto the

mica-coated silicon wafer. The evaporation might have caused the sheets to aggregate causing an inhomogeneous surface height distribution. To overcome this problem, it might be necessary to drop-cast the BP dispersed in NMP or DMPU directly onto the wafer. However, due to the high boiling point of either solvent (> 200 °C), the evaporation of the solvent is challenging and time-consuming.

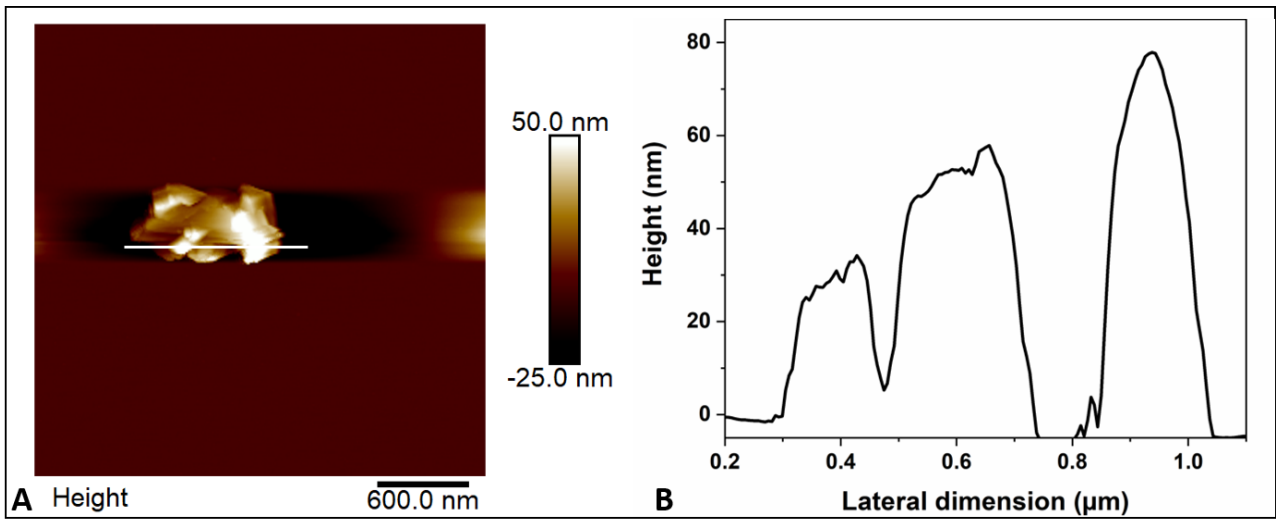

Figure 7 – AFM of exfoliated BP. **A:** AFM image of BP exfoliated in NMP. **B:** Height profile of indicated straight line from **A**. Image shows severe restacking and aggregation of sheets due to sample preparation.

Zeta potential analysis showed -36 mV for both exfoliation batches, showing that there is no difference in the surface structure of either material. The highly negative charge arises from the P-O bond on the surface of the nanosheets after being dispersed in water.[55]

As shown before, BP is IR inactive. Due to the mutual exclusion rule, it, therefore, is Raman active. The reason why BP is Raman active is the change in the polarizability of the bonds upon irradiation of the sample using laser light. The three distinct and characteristic Raman peaks for BP corresponding to the vibrational modes (fig. 8 C) are A^1_g (361 cm^{-1}), B_{2g} (438 cm^{-1}) and A^2_g (466 cm^{-1}). To determine, whether the Raman spectrum of BP changes after exposing the samples to air, the measurement was performed after three different exposure times (0 hours, 3 days and 8 days). All obtained spectra were normalized to the silicon peak from the used wafer at 521 cm^{-1} and show the three characteristic Raman peaks for BP (fig. 8 A & B). An indication for the oxidation of the BP nanosheets can be obtained from the integrated peak ratios of the A^1_g peak to the A^2_g peak. If the ratio A^1_g / A^2_g < 0.2, the BP sheets are significantly oxidised for a sheet thickness of up to 10 nm.[26] The integrated peak ratios for the BP exfoliated in NMP are significantly lower than the ones for BP exfoliated in DMPU, suggesting that DMPU might be better able to shield the nanosheets from oxygen and water (table 1).

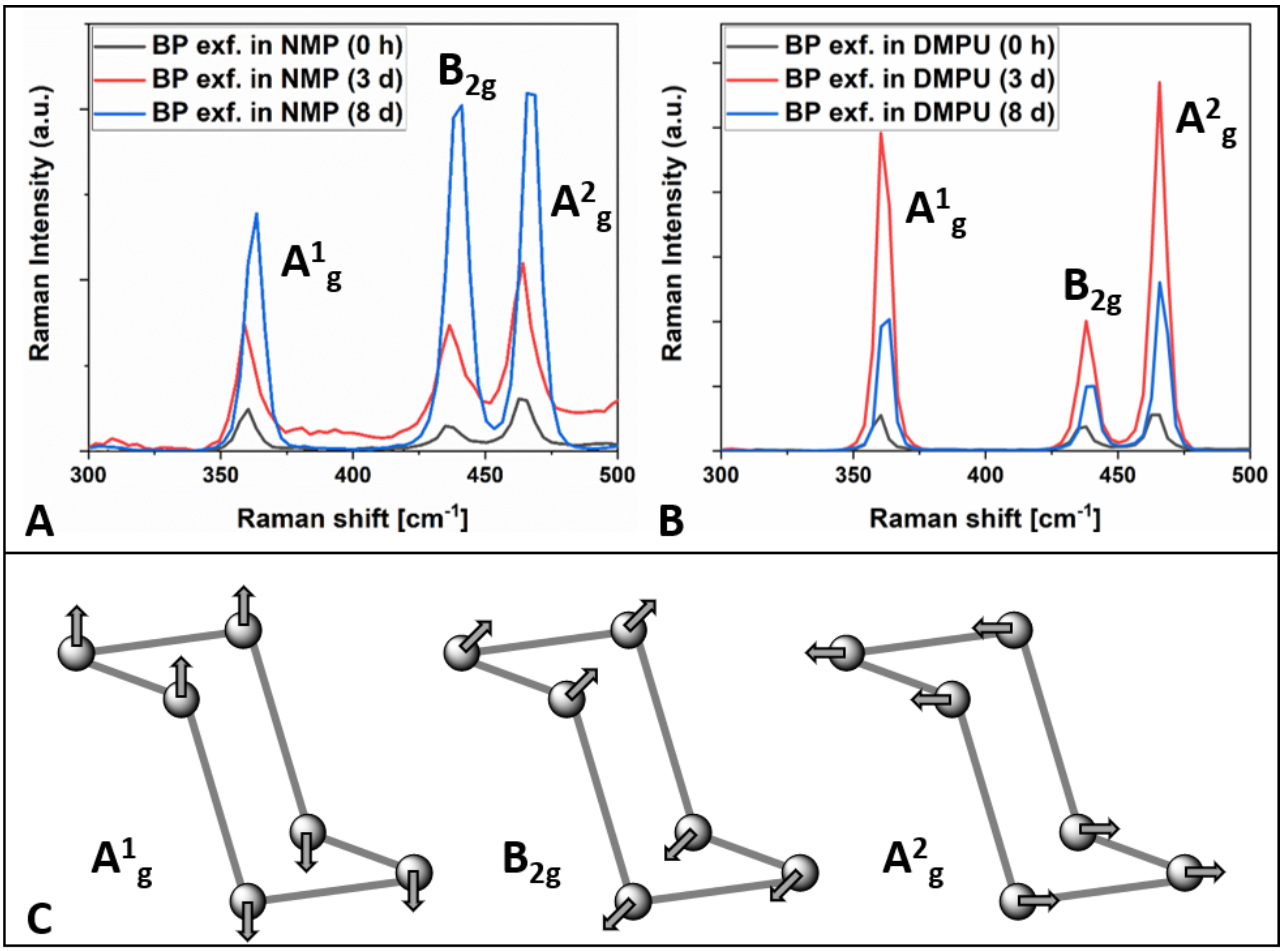

Figure 8 – Raman spectroscopy of exfoliated BP. **A:** BP exfoliated in NMP. **B:** BP exfoliated in DMPU. The spectra were obtained after an exposure of the samples to air for 0 hours, 3 days and 8 days, respectively. **C:** Schematic representation of Raman modes for BP.

Table 1 – Raman spectroscopy: Integrated peak ratios of A^1_g / A^2_g after air exposure for different time frames.

Exposure to air	BP exfoliated in NMP	BP exfoliated in DMPU
0 h	**0.72**	**0.88**
3 d	**0.70**	**0.79**
8 d	**0.57**	**0.74**

The exfoliation of BP nanosheets was successful in both NMP and DMPU with no evident differences. Both solvents yielded comparable amounts of FTIR inactive and non-oxidised BP nanosheets with lateral sizes ranging from 100 nm to 1 µm. Only the Raman analysis suggests that DMPU might be better able to shield the sheets from oxygen and water which is supported by previous publications.[26]

Functionalization of BP using a co-polymerization of L-lactide and glycidol

The functionalization aimed to obtain water-soluble and biodegradable BP nanosheets that are suitable for biomedical applications such as photothermal therapy. Therefore, the previously exfoliated BP was functionalized using a one-pot ring-opening co-polymerization of L-lactide and glycidol under inert conditions. The polymerization was performed either in a one-step reaction, by adding all components directly to the reaction mixture, or in two steps by first adding L-lactide to BP and later adding glycidol. It was expected that the product of the two-step reaction would show a better water-solubility, as the hydrophilic PG groups would be expected on the surface of the product. Both reactions were operated in NMP and DMPU to compare the suitability of the solvents for the functionalization of BP. After the polymerization, dark brown to black dispersions were obtained for all reactions (fig. 9).

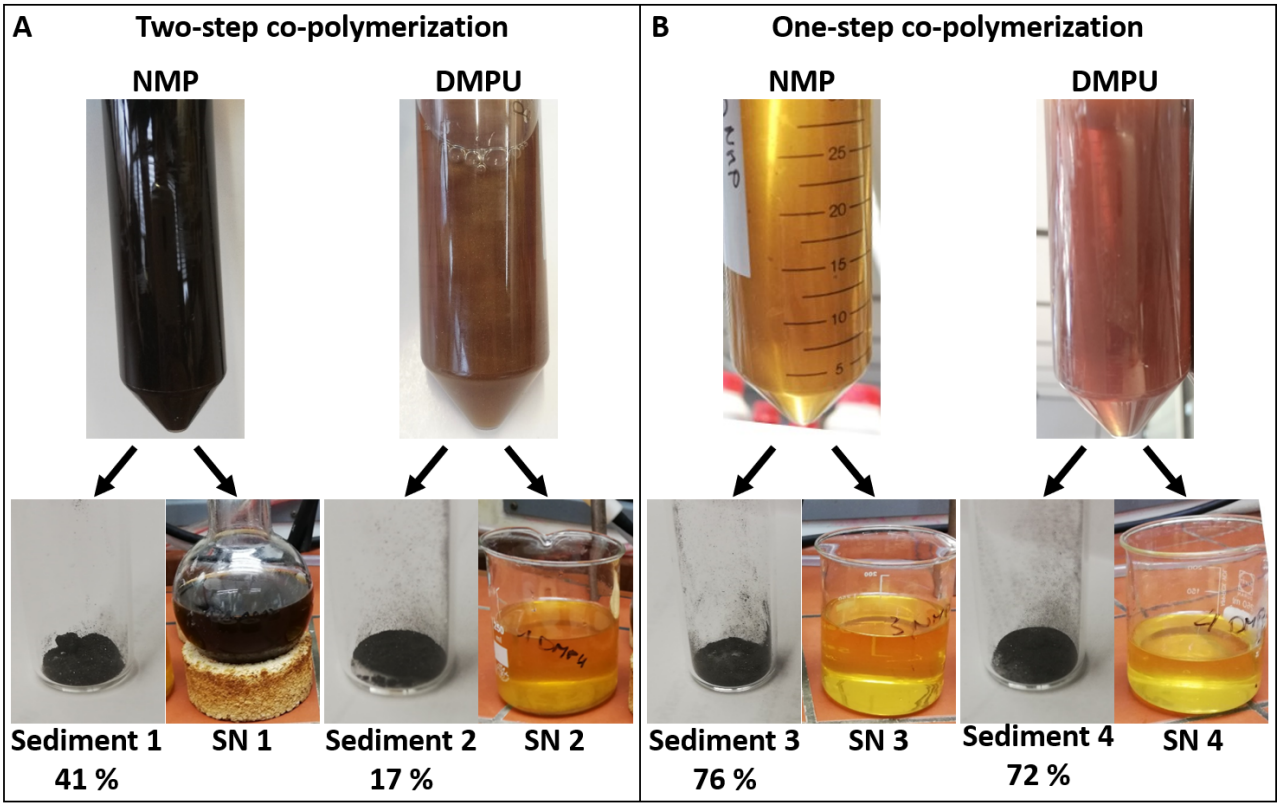

Figure 9 – Functionalization of BP. Top row: Reaction mixtures immediately after the reaction. Bottom row: lyophilized sediments of each reaction after all centrifugation steps (three times in DMF/MeOH, then three times in water) and all collected supernatants (SN) of all centrifugation steps. **A:** Two-step co-polymerization in NMP and DMPU. **B:** One-step co-polymerization in NMP and DMPU.

Assuming that the functionalized BP sheets would sediment upon centrifugation due to the high molecular weight, the reaction mixtures were centrifuged several times in

DMF/MeOH and several times in water to remove the catalyst and residual monomers. The sediments of all reactions showed no apparent difference (fig. 9), but rather looked like exfoliated BP (fig. 4 D). FTIR analysis revealed that there was no functionalized BP present in the sediment of any reaction because peaks that indicate the presence of polylactide or hPG were not found in the IR spectrum of any sediment (fig. 10). However, the FTIR spectra show a higher degree of oxidation (peak at 1000 cm^{-1}) for the sediments compared to exfoliated BP which is probably caused due to the exposure to ambient conditions during the centrifugation steps.[18][29]

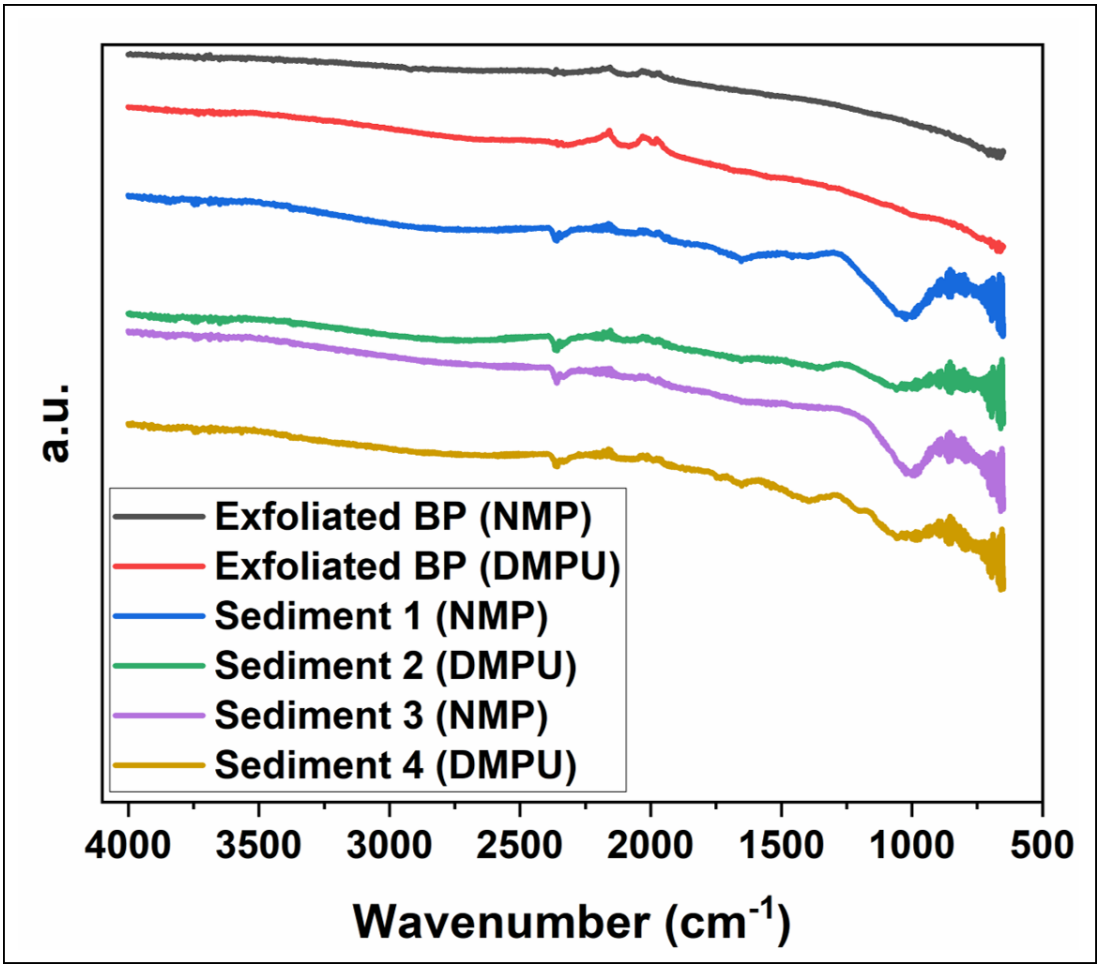

Figure 10 – FTIR spectra of the sediments after functionalization (compare fig. 9).

The supernatants of all centrifugation steps were collected and since the supernatant of the two-step co-polymerization in NMP appeared to be deeply black (fig. 9 SN1), it was expected that there was a large amount of BP dissolved in the mixture. Therefore, the supernatant was dialysed thoroughly against water and lyophilised. Due to the expected much lower yields of the other supernatants, it was renounced on dialysing them as well. Comparing the performed reactions, it can be concluded that NMP is more convenient for the functionalization of BP nanosheets with these polymers and that the two-step reaction seems more favourable than the one-step co-polymerization.

Since the FTIR spectrum of the obtained product from supernatant 1 (BP-PLA-PG (1:1)) indicated the presence of polymer (fig. 12), the same reaction was repeated with an increased amount of glycidol aiming to increase the water-solubility of the product. Instead of using a 1:1 monomer ratio of L-lactide to glycidol, the ratio was increased to 1:2 (BP-PLA-PG (1:2)). For this reaction, the supernatant after all centrifugation steps was deeply black as well (fig. 11 D). Therefore, the mixture was dialysed against water and lyophilized. BP-PLA-PG (1:1) appeared to be a dry solid but BP-PLA-PG (1:2) rather had a honey-like consistency (fig. 11 B & E) which is probably caused by a higher hPG content. Both products exhibited a high water-solubility (fig. 11 C & F) without visible changes even after several weeks in solution. Assuming that all BP that did not sediment was functionalized, BP-PLA-PG (1:1) consists of 31.7 mg polymer and 5.9 mg exfoliated BP, while BP-PLA-PG (1:2) contains 36 mg polymer and 5.0 mg exfoliated BP.

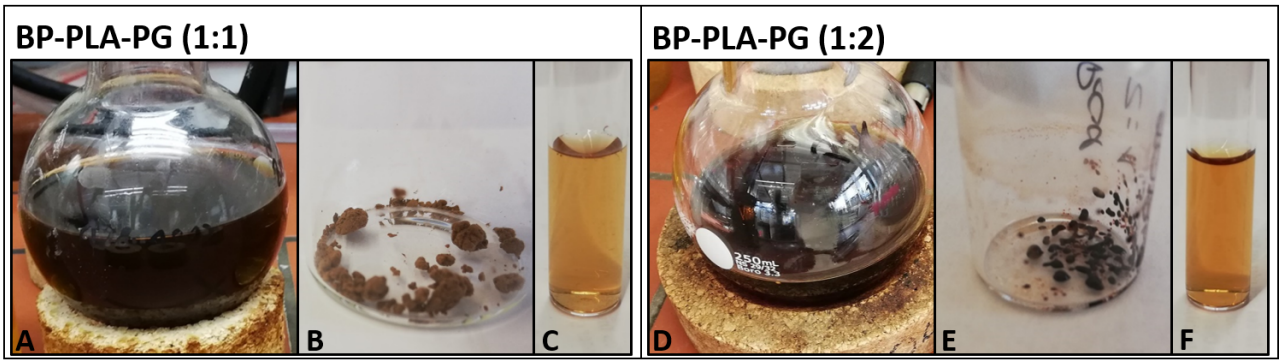

Figure 11 – BP-PLA-PG (1:1) and (1:2). **A:** Supernatant after all centrifugaton steps. **B:** Lyophilized product (36.6 mg). **C:** BP-PLA-PG (1:1) dissolved in water. **D:** Supernatant after all centrifugaton steps of BP-PLA-PG (1:2). **E:** Lyophilized product (41.0 mg). **F:** BP-PLA-PG (1:2) dissolved in water.

FTIR analysis revealed the presence of polymer in BP-PLA-PG (1:1) and (1:2). The IR spectra of BP-PLA-PG (1:2) showed a higher similarity to hPG, while BP-PLA-PG (1:1) exhibited properties closer to polylactide (fig. 12). The peak from 3100 to 3600 cm^{-1} can be assigned to the O-H stretching of PG. The strong peak at 1050 cm^{-1} can be assigned to ester bonds or primary alcohols while the peak at 1450 cm^{-1} corresponds to C-H bonds. The peak at 1600 cm^{-1} can be assigned to carbonyl groups. However, both products were water-soluble and could be re-dissolved in water even after lyophilization easily.

Table 2 – Surface Zeta Potential measured in water.

Sample	Surface Zeta Potential [mV]
Exfoliated BP	**-36**
BP-PLA-PG (1:1)	**-20**
BP-PLA-PG (1:2)	**-16**

According to zeta potential measurements, the surface charge of BP was decreased upon functionalization (table 2) for both products which is caused by the shielding effect of the polymers on top of the BP surface. The negative charge arises from the terminal alcohol groups.

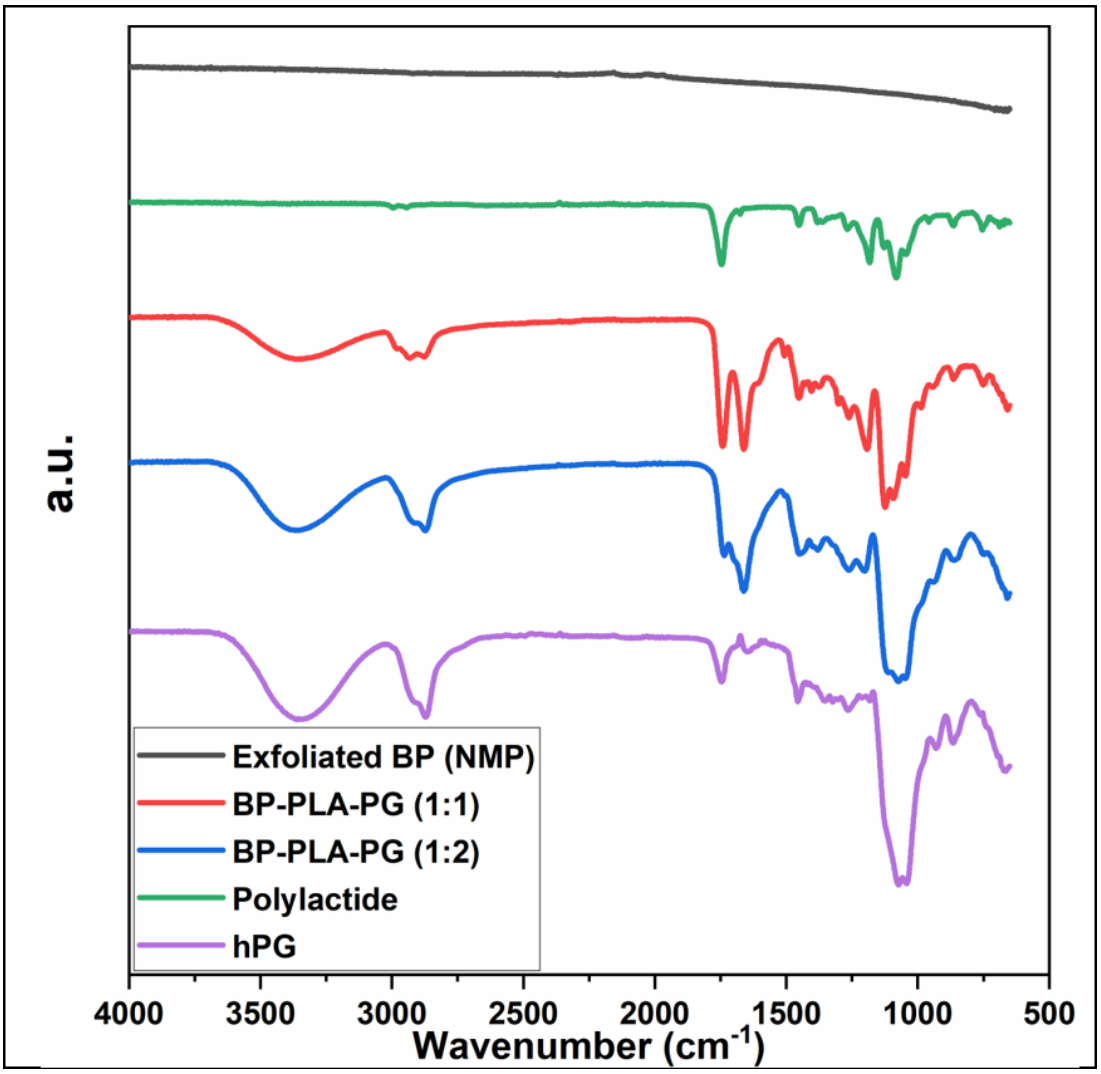

Figure 12 – FTIR of BP-PLA-PG (1:1) and (1:2) as well as hPG and polylactide.

To get an insight into the overall structure of the products, TEM analysis was performed on at least 16 sheets per sample. As it was assumed that the functionalization would increase the stability of the products in water, the samples were kept in water several days before the measurement. However, BP-PLA-PG (1:1) appeared to be rather unstable in water, as the obtained TEM images show the presence of BP sheets that contain many holes and are severely degrading (fig. 13 A & B). BP-PLA-PG (1:1) was kept in water for 6 days while BP-PLA-PG (1:2) was kept in water for 3 days prior to the measurement. However, BP-PLA-PG (1:2) as well shows signs of degradation indicated by the formation of bubbles on the surface (fig. 13 C & D). The reason for the high reac-

tivity of the functionalized sample probably arises from the P-C=O bond at the surface of the BP sheets. Due to resonance structures, water acting as a nucleophile can easily attack the P-C bonds which leads to the degradation of the BP sheet.[29] However, these images confirm lateral sizes of the sheets ranging from 100 nm to 1 µm which is consistent with the non-functionalized sheets.

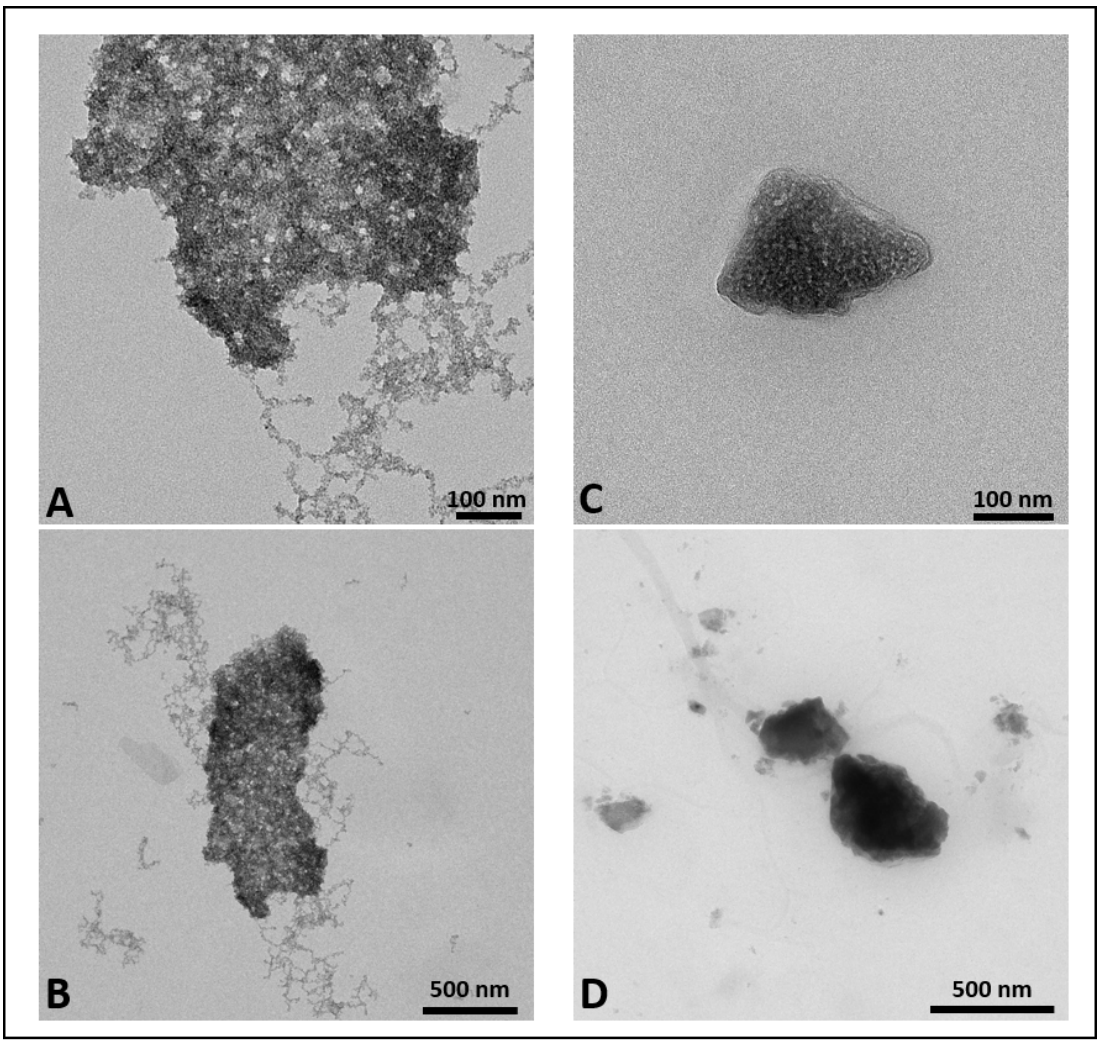

Figure 13 – TEM of BP-PLA-PG (1:1) and (1:2). **A & B:** BP-PLA-PG (1:1) showing highly degraded BP nanosheets. **C & D:** BP-PLA-PG (1:2) with a decreased degree of degradation.

For BP-PLA-PG (1:1), additional AFM images were obtained (fig. 14). In total, three flakes were analysed which confirm the instability of the sample in water. The height profile shows an average height of 32 nm and an inhomogeneous surface roughness. Furthermore, there seems to be a plateau at 30 nm which is to be expected for a 2D material. Since the sample was drop-casted while being dissolved in water, the evaporation of the solvent is slower than it is for ethanol. This fact probably prevents the restacking of the sheets which was a major problem faced for the sample preparation of the non-functionalized sample. Furthermore, the lateral sizes revealed by AFM analysis are in

the same range as suggested by the obtained TEM images. To get an insight into the polymer composition of both samples, proton NMR was performed in D_2O (fig. 21). In the ^1H NMR spectrum, signals from 2.0 to 2.25 ppm are attributed to the methylene protons in the lactide segments, while the signals at 4.66 ppm are attributed to the protons next to the ester bond in the lactide segments. Signals from 3.4 to 4.2 ppm correspond to the polyglycerol segments. Comparing the integrated signals yields that BP-PLA-PG (1:1) contains a significantly larger amount of lactide segments (about 25 times more) than glycerol segments whose signals are very weak. BP-PLA-PG (1:2) contains about 13 times more lactide segments than glycerol segments (fig. 21).

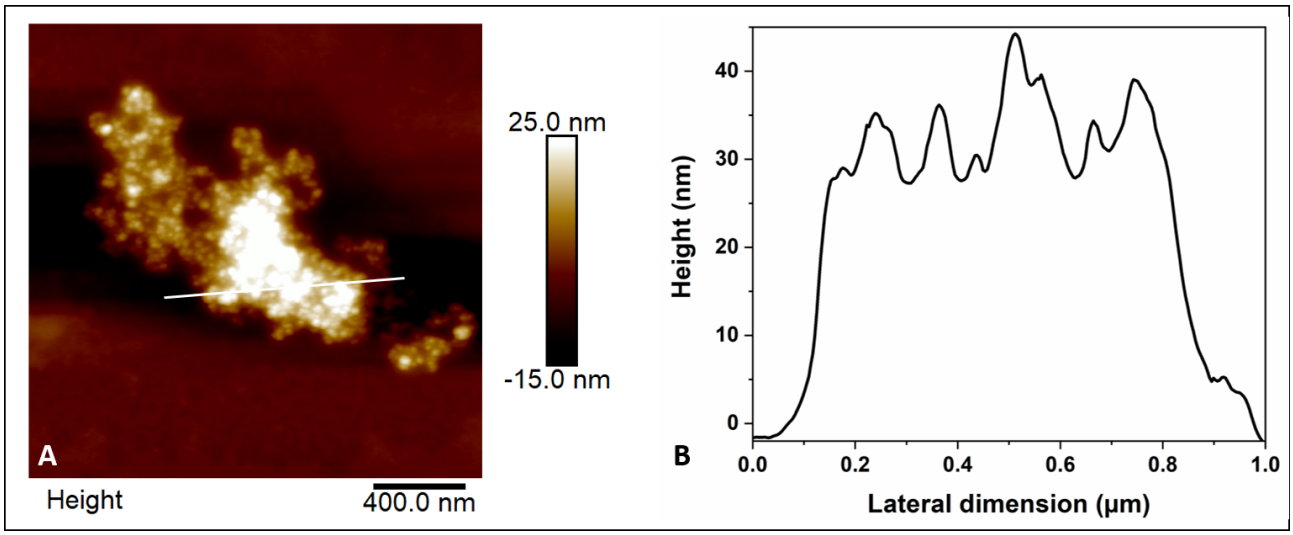

Figure 14 – AFM of BP-PLA-PG (1:1). **A:** BP-PLA-PG (1:1) showing highly degraded BP nanosheets. **B:** Height profile of indicated line in **A**.

TGA of both products confirms that BP-PLA-PG (1:1) is thermally less stable than BP-PLA-PG (1:2). Furthermore, TGA reveals that BP-PLA-PG (1:2) contains about 80 % of polymer, while BP-PLA-PG (1:1) contains only 30 % polymer, assuming that BP does not burn before 500 °C (fig. 13 E).

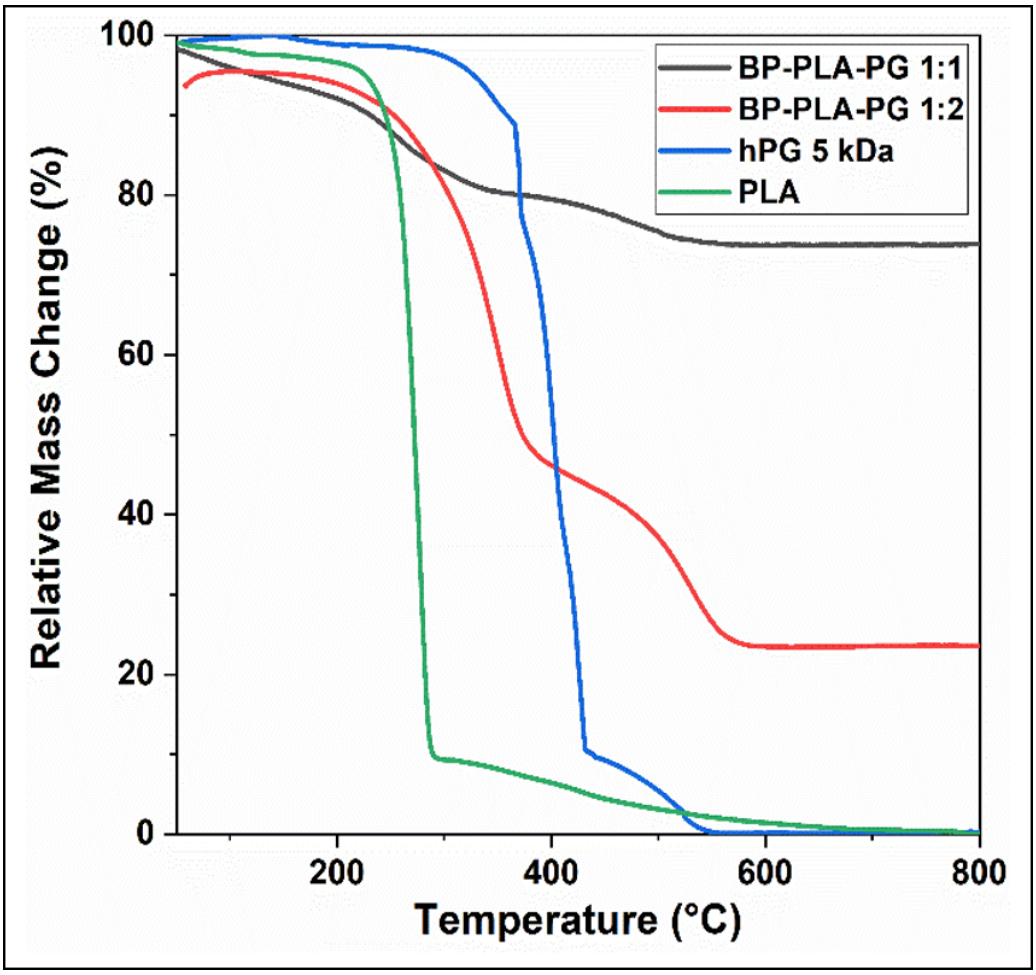

Figure 15 – TGA of BP-PLA-PG (1:1) and (1:2), as well as hPG and polylactide as reference.

After looking at all the obtained data, it is possible to conclude that the functionalization of BP nanosheets using a one-pot ring-opening co-polymerization of L-lactide and glycidol was successful. Comparing NMP and DMPU as solvents for the functionalization revealed that using DMPU presumably yields much less functionalized BP sheets, while the functionalization in NMP was successful. Furthermore, using equimolar monomeric ratios of lactide and glycidol resulted in water-soluble and degradable BP nanosheets while doubling the amount of glycidol yields water-soluble and thermally more stable BP sheets. BP-PLA-PG (1:2) exhibits properties that are similar to the ones of hPG such as a honey-like consistency and FTIR spectrum. The lateral sizes of the functionalized BP sheets are consistent with the sheet sizes of the non-functionalized BP and range from 100 nm to 1 µm with heights up to 40 nm. Comparing these results with previous studies on BP, the low stability of the sheets upon functionalization was not expected.[56] Many studies reported stability under ambient conditions of several months after functionalization.[31] However, looking at the resonance structures of the synthesized material, the degradation in water is comprehensible.[29]

In-vitro assays for biomedical applications

The last step of the project aimed to test the suitability of the obtained products BP-PLA-PG (1:1) and (1:2) for biomedical applications. For that purpose, the photothermal properties were studied as well as the drug loading capacity and the overall toxicity of the samples on living cells. To test whether the functionalized BP is suited for photothermal therapy, the absorption of the samples was measured using UV-Vis (fig. 16 A). BP-PLA-PG (1:1) showed a slightly higher absorption at 785 nm which is the wavelength of the laser for the photothermal test. Therefore, BP-PLA-PG (1:1) is expected to show higher photothermal efficiency. BP showed a high absorption at a wavelength of 785 nm and thus exhibited an efficient photothermal effect reaching temperatures of up to 55 °C (fig. 16 B). However, the difference in the photothermal efficiency might arise from the significantly decreased concentration of pristine BP in the functionalized samples. BP-PLA-PG (1:1) contains 16.1 % of pristine PB while BP-PLA-PG (1:2) contained 12.1 % of pristine BP. For future studies, it would be necessary to adapt the concentrations of the samples to equal amounts of BP. Therefore, the present data only showed qualitatively that the functionalized samples show an efficient photothermal effect.

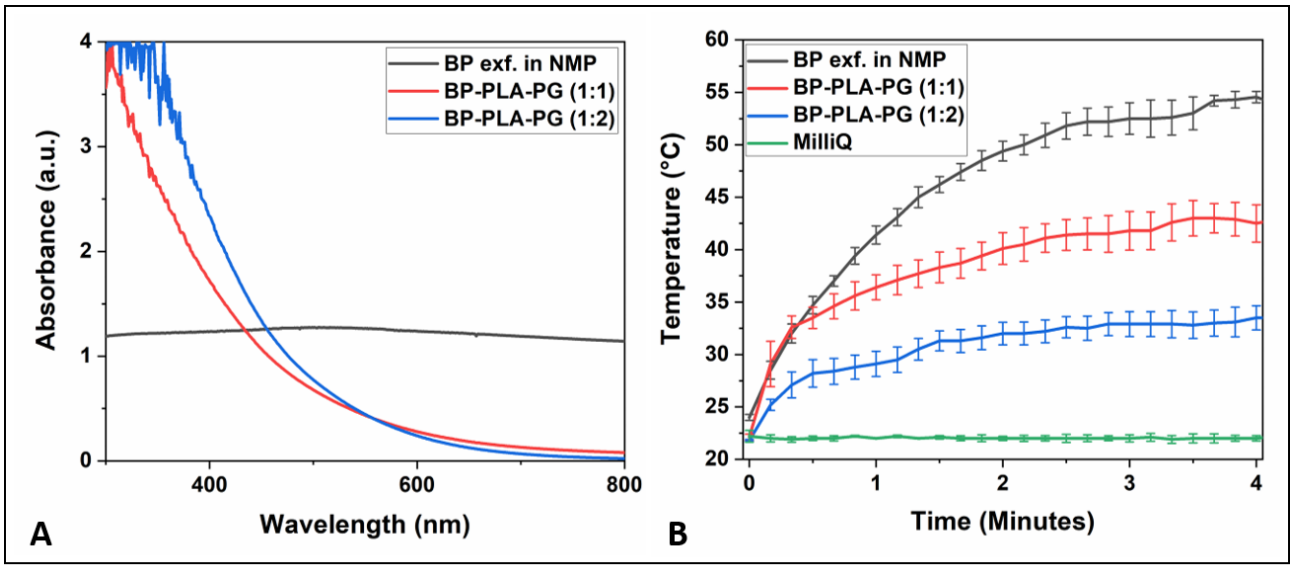

Figure 16 – Photothermal effect. **A:** UV-Vis spectrum of pristine BP and the functionalized samples. (Measured at 0.25 mg/mL) **B:** Photothermal effect of pristine BP (2 mg/mL) and functionalized BP (3 mg/mL). water was measured as negative control.

The drug loading capacity of pristine BP and the functionalized samples was determined using doxorubicin which is a commonly used cytostatic drug used for chemotherapy. Doxorubicin is a cationic drug which is absorbed by a surface due to electrostatic interactions. Due to the highly negative surface zeta potentials of the BP samples (table 2), a superior drug loading efficiency was expected. Therefore, the absorbance of

different concentrations of doxorubicin at 480 nm was measured (fig. 17 A) and a calibration curve relating the doxorubicin concentrations to the absorbance was obtained (fig. 17 B). Using this calibration curve, the amount of doxorubicin loaded onto the BP samples was determined, yielding a drug loading capacity of 16.3 % for exfoliated BP. BP-PLA-PG (1:1) showed a drug loading capacity of 14.1 % while BP-PLA-PG (1:2) showed the lowest loading capacity of 8.3 % (table 3).

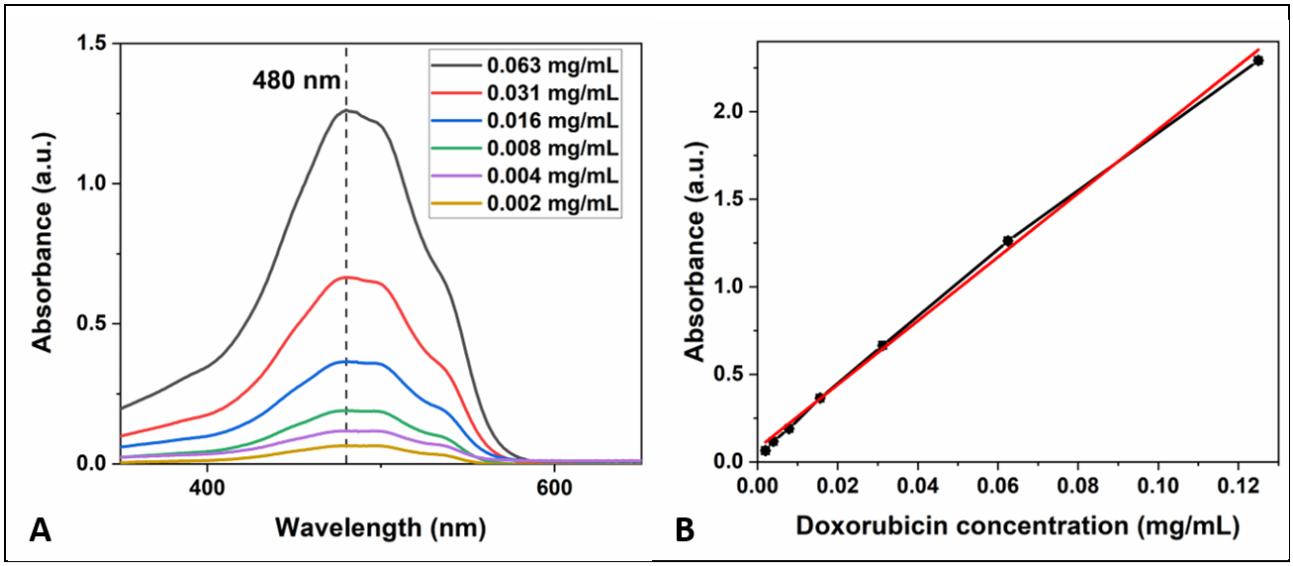

Figure 17 – Drug loading calibration. **A:** UV-Vis spectroscopy of doxorubicin in water at six different concentrations. **B:** Calibration curve of doxorubicin concentrations related to the measured absorbance at 480 nm. Linear fit: Slope 18.21, intercept 0.077.

Table 3 – Doxorubicin loading capacity of exfoliated BP and functionalized BP nanosheets.

Sample	Compound [mg]	Loaded Drug [mg]	Loading Capacity [%]
Exf. BP	**2**	**0.327**	**16.3**
BP-PLA-PG (1:1)	**3**	**0.424**	**14.1**
BP-PLA-PG (1:2)	**3**	**0.248**	**8.3**

Both, the non-functionalized BP and the functionalized BP have been incubated with human HeLa cells as well as bacterial cells to determine the toxicity of the samples. HeLa cells were chosen as they are very convenient to culture and give highly reliable results for the toxicity of a given compound. The CCK8 cell viability assay is a colorimetric assay based on the reduction of tetrazolium salt to a formazoan dye which is performed by dehydrogenases in living cells. The absorption at 460 nm is directly proportional to the number of living cells. The live-dead staining is based on the fluorescence of ethidium homodimer and calcein-AM. Green fluorescent calcein-AM indicates the presence of intracellular esterase activity and thus stains the living cells, while red fluorescent

ethidium homodimer indicates a disrupted plasma membrane and thus stains dead cells.

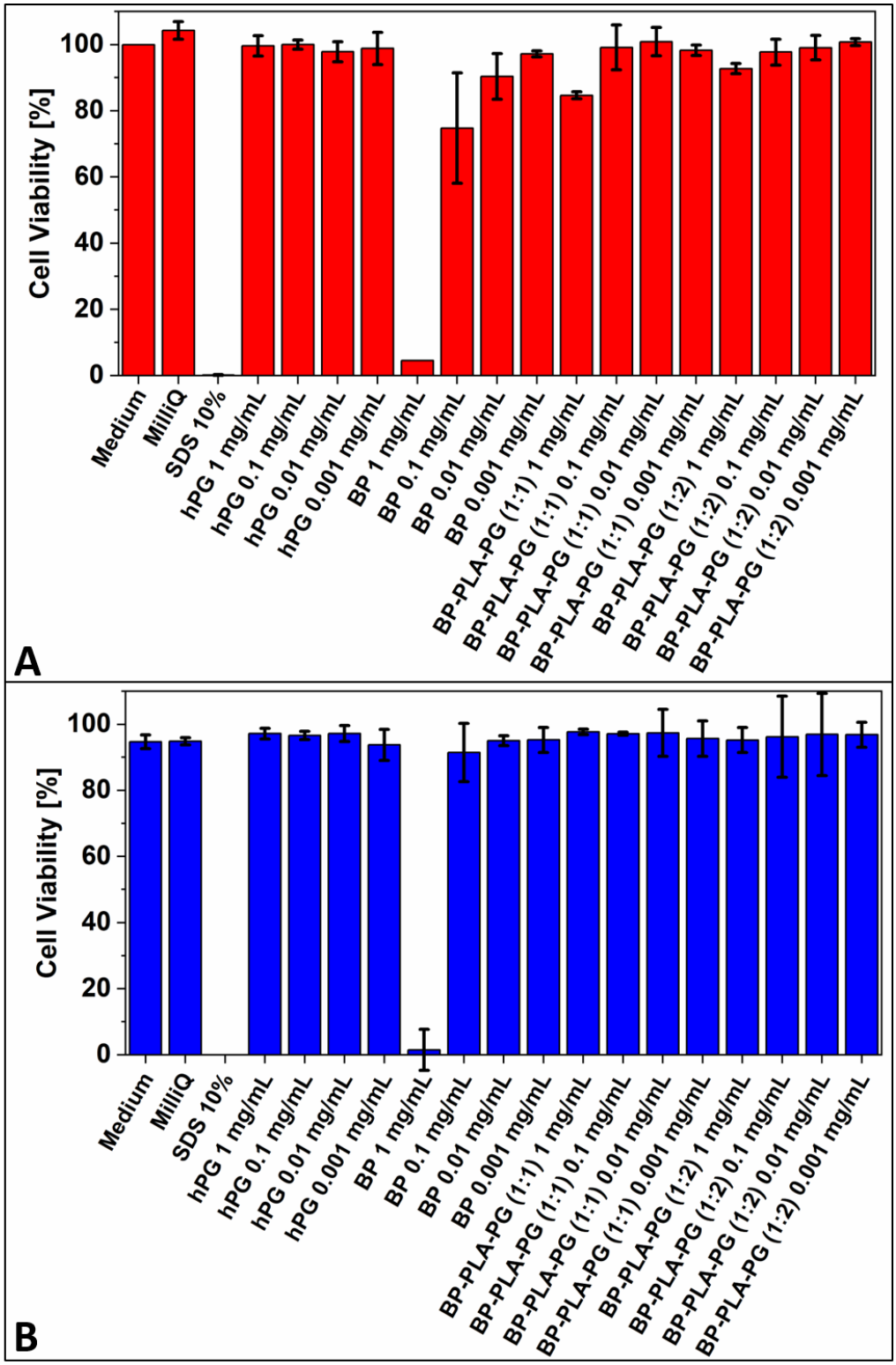

Figure 18 – Cell viability assay. **A:** Cell viability determined using CCK8 solution. Values are normalized to the medium reference. **B:** Cell viability determined using live-dead staining. In both cases, SDS has been used as negative control.

The results of the CCK8 assay and the live-dead staining method are consistent with each other showing low cell viability for non-functionalized BP at high concentrations and tremendously increased cell viability after functionalization at the same concentration (fig. 18 A & B). The images obtained by fluorescence microscopy from the live-dead staining show a high number of dead cells for pristine BP at high concentrations while the functionalized samples predominantly show living cells (fig. 19). The bright-field images show a tremendous coverage of BP for the non-functionalized sample suggesting that either sharp edges of the sheets disrupt the cell membranes or that the formation of phosphoric acid due to the long incubation time has a toxic effect on the cells.[55] From these results, it is possible to conclude that the functionalization does not only make the compounds water-soluble but also reduces the toxicity of BP drastically.

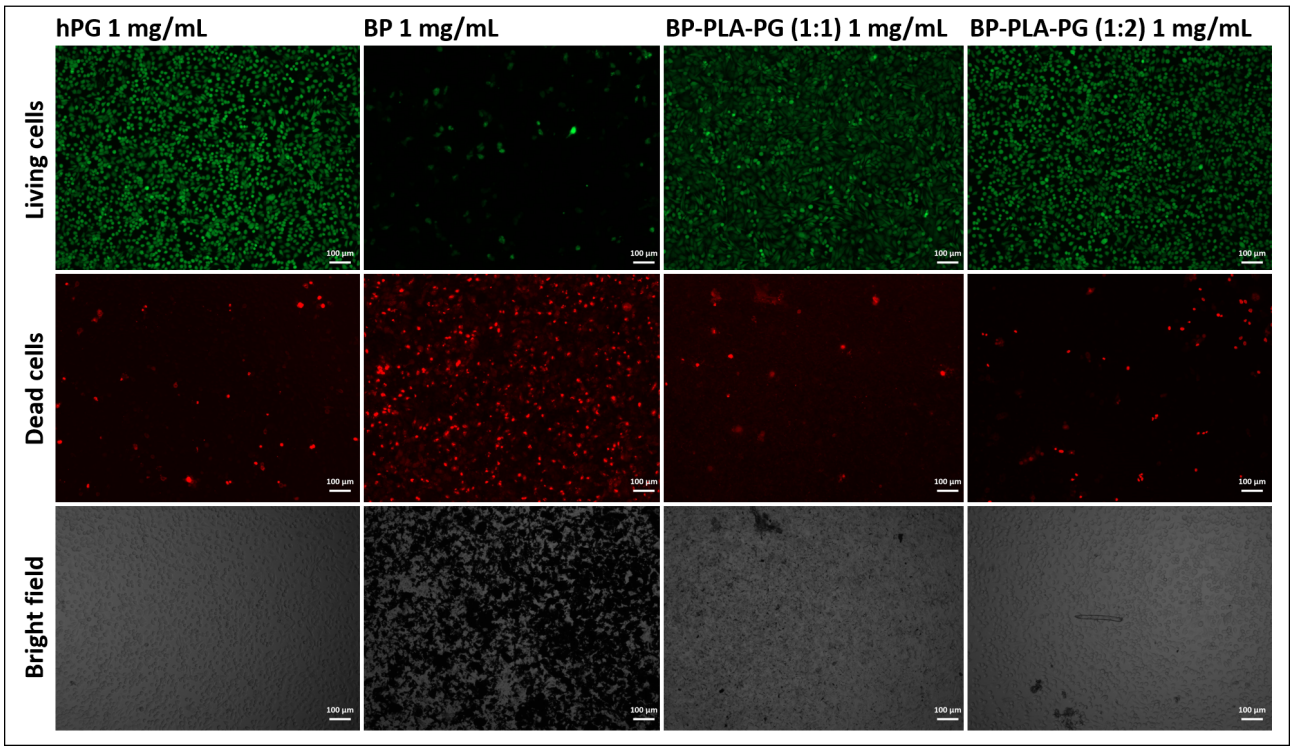

Figure 19 – Fluorescence images of the live-dead staining. Green-coloured are the living cells, while red colour indicates dead cells. Scale bars: 100 µm.

To test whether there is any antimicrobial effect of BP upon functionalization, the BP-PLA-PG (1:1) and (1:2) were incubated with E. Coli bacteria and the colony-forming units (CFU) were determined. The results do not show an antimicrobial effect, but they confirm that pristine BP at high concentrations is more toxic than the functionalized BP nanosheets (fig. 20).

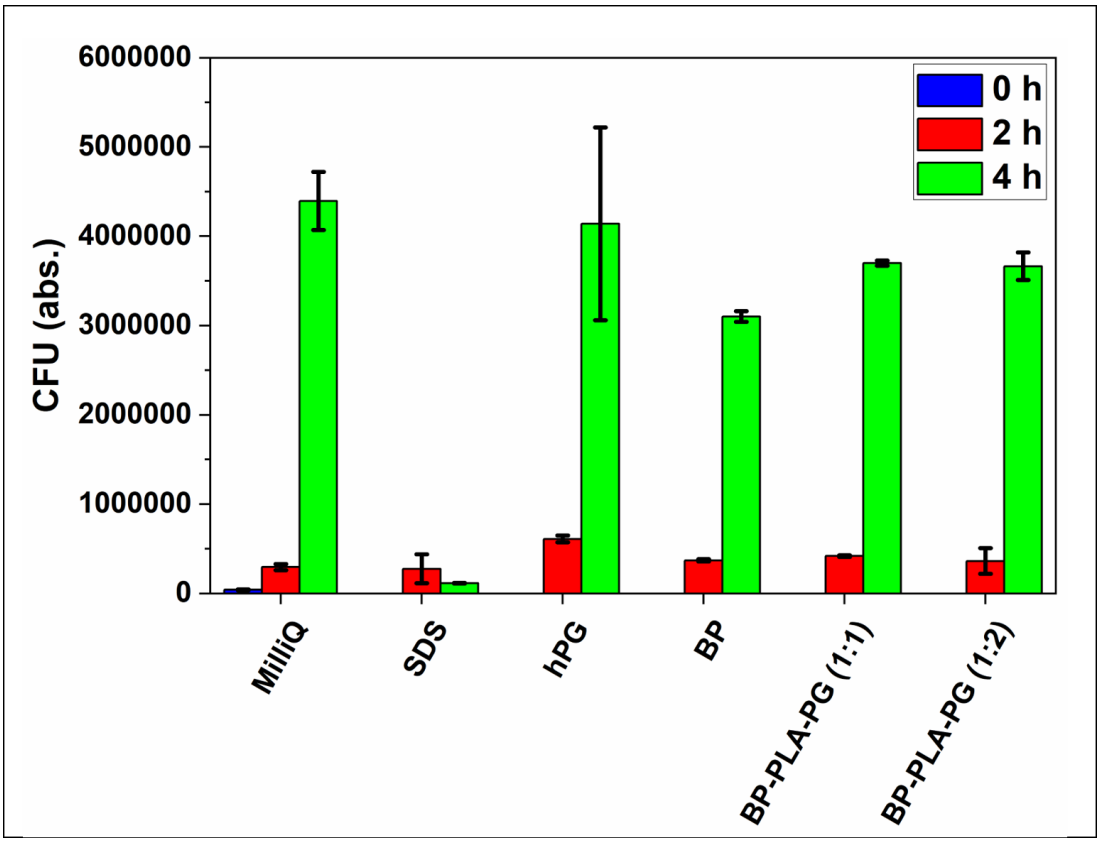

Figure 20 – Antimicrobial assay. CFUs were counted after incubating the bacteria with the respective sample for the indicated period of time.

From these results, it can be concluded that BP has a high photothermal efficiency which was also reported in many publications. Upon functionalization, the samples still showed a good photothermal effect. Due to a smaller amount of BP in the functionalized samples, it was not possible to quantify the differences in efficiency. For a quantitative determination, the overall amount of BP in each sample would need to be equal. However, the preliminary results confirmed that BP-PLA-PG (1:1) and (1:2) might be suitable agents for photothermal therapy. Furthermore, both samples showed a high doxorubicin loading capacity and a significantly reduced toxicity compared to pristine BP. Although BP nanosheets ought to be non-toxic as reported in literature,[1][20] the toxicity is dependent on the sheet size and the incubation time. Sharp edges of the sheets and the formation of phosphoric acid might be a reason for the high toxicity of BP.[29][48][55] However, since BP-PLA-PG (1:1) and (1:2) showed low toxicity, good photothermal effect and a high drug loading capacity, they are promising candidates for biomedical applications.

Conclusion and outlook

The liquid phase exfoliation of BP in NMP and DMPU was successful and yielded BP nanosheets with lateral sizes up to one µm and several nm in thickness. There was no apparent difference in the quality of the sheets after exfoliation in either solvent. From that, it can be concluded that both are suitable solvents for the liquid phase exfoliation of BP. However, Raman analysis suggested that DMPU was better able to shield the sheets from degradation.
Furthermore, it was possible to functionalize the nanosheets with a co-polymer consisting of lactide and glycerol segments. The functionalized material showed a good water-solubility and a significantly reduced toxicity towards human and bacterial cells. The comparative study between NMP and DPU as solvents for the functionalization showed that NMP was much more convenient compared to DMPU.
Comparing two different monomer ratios of glycidol and lactide yielded that BP-PLA-PG (1:1) was better suited for photothermal therapy and showed a higher drug loading capacity.

For future studies, it is necessary to prove the covalent functionalization using XPS and solid-state NMR. Furthermore, the degradation after functionalization is of major importance and need to be observed over a longer period of time. Drug release studies with and without IR irradiation needs to be tested *in-vitro*, as well as the cellular uptake process to comprehend the effect of the compound on the cells in detail. However, it can be concluded that BP and its functionalized analogues are a novel class of materials exhibiting highly promising properties for biomedical applications.

Acknowledgements

I would like to show my gratitude to everyone who supported and helped me during the time of my master's thesis.
First, I would like to thank Prof. Dr. Rainer Haag for providing the opportunity of joining his research group and for the possibility to participate in current research.
Many thanks, I want to devote to Prof. Dr. Mohsen Adeli for the opportunity of working on BP and for his patient support during the project. I very much appreciated the help. Furthermore, I would like to thank Dr. Katharina Achazi for the coordination of the project and the helpful insights on the biological part of the project.
Special thanks I would like to devote to Dr. Ievgen Donskyi for his support during the project and the many highly appreciated discussions on how to work with two-dimensional nanomaterials and the guidance and help during the project.
Next, I would like to express my gratitude towards Dr. Svenja Ehrmann for the TEM imaging, Rameez Ahmed for the AFM images, Yannic Kerkhoff (AG Block) for the help with the image analysis and Dr. Georgy Gordeev (AG Reich) for providing the Raman spectra. I highly appreciated all the time and effort that was spent to support me during the project.
Many thanks, I would like to devote to the people from the biolab for their kind support and for spending so much time together. In particular, I want to thank Elisa Quaas and Scarlett Manzke for teaching me the art of cell culturing and for their help during the project.
Furthermore, I would like to thank the members of my chemistry lab for the great time in the lab and for answering all my sometimes maybe stupid questions. Special thanks, I want to devote to Obida Bawadkji for helping me get around in the lab and for the helpful insights in the work with BP. I highly appreciated the discussions on the project and the advice he provided.
Next, I want to thank Dr. Ehsan Mohammadifar for providing the polylactide and Dr. Mathias Dimde for providing the distilled glycidol which saved me much time and effort.
Many thanks, I want to devote to everyone from the AG Haag for welcoming me openly and for the great time I had while working on the project. I will always remember the group events such as the group trip, the cocktail evenings, the Christmas party and the visits to Christmas markets, as well as the casual lunch times.
I would like to acknowledge the assistance of the Core Facility BioSupraMol supported by the DFG.
Last, I want to thank friends from the undergraduate program for their support during the difficult lectures and for the great times spent together at the university and various other occasions.

My deepest thanks, I would like to devote to my family for their love and support and for having my back during all ups and downs of life and for being there when I need it most.

I would like to show my gratitude to the Swiss Nanoscience Institute for the generous Nanoscience Argovia Travel Grant.

References

[1] Anju, S., Ashtami, J. & Mohanan, P. V. Black phosphorus, a prospective graphene substitute for biomedical applications. Materials Science and Engineering: C 97, 978–993 (**2019**).

[2] Zhang, H. Ultrathin Two-Dimensional Nanomaterials. ACS Nano 9, 9451–9469 (**2015**).

[3] Rafiei-Sarmazdeh, Z., Zahedi-Dizaji, S. M. & Kang, A. K. Two-Dimensional Nanomaterials. in Nanostructures (IntechOpen, **2019**).

[4] Zhu, J. et al. The rapid emergence of two-dimensional nanomaterials for high-performance separation membranes. Journal of Materials Chemistry A 6, 3773–3792 (**2018**).

[5] Wu, S., Hui, K. S. & Hui, K. N. 2D Black Phosphorus: from Preparation to Applications for Electrochemical Energy Storage. Advanced Science 5, 1700491 (**2018**).

[6] Zhong, Y., Zhen, Z. & Zhu, H. Graphene: Fundamental research and potential applications. FlatChem 4, 20–32 (**2017**).

[7] Geim, A. K. & Novoselov, K. S. The rise of graphene. in Nanoscience and technology: a collection of reviews from nature journals 11–19 (World Scientific, **2010**).

[8] Novoselov, K. S. et al. A roadmap for graphene. Nature 490, 192–200 (**2012**).

[9] Lalwani, G., D'Agati, M., Khan, A. M. & Sitharaman, B. Toxicology of Graphene-Based Nanomaterials. Adv Drug Deliv Rev 105, 109–144 (**2016**).

[10] Li, L. et al. Black phosphorus field-effect transistors. Nature nanotechnology 9, 372 (**2014**).

[11] Xu, X. et al. Coherent Optical Spectroscopy of a Strongly Driven Quantum Dot. Science 317, 929–932 (**2007**).

[12] Yang, T. et al. Atomically Thin 2D Transition Metal Oxides: Structural Reconstruction, Interaction with Substrates, and Potential Applications. Advanced Materials Interfaces 6, 1801160 (**2019**).

[13] Balendhran, S., Walia, S., Nili, H., Sriram, S. & Bhaskaran, M. Elemental analogues of graphene: silicene, germanene, stanene, and phosphorene. small 11, 640–652 (**2015**).

[14] Vogt, P. et al. Silicene: Compelling Experimental Evidence for Graphene-like Two-Dimensional Silicon. Physical Review Letters 108 (**2012**).

[15] Lin, T. et al. Nitrogen-doped mesoporous carbon of extraordinary capacitance for electrochemical energy storage. Science 350, 1508–1513 (**2015**).

[16] Smart-elements GmbH. http://www.smart-elements.com/wp/. (Access: Nov. **2019**).

[17] Two-dimensional phosphorus reveals unexpected superconducting behaviour. The Engineer https://www.theengineer.co.uk/two-dimensional-phosphorus-reveals-unexpected-superconducting-behabviour/ (**2017**). Access: Nov. 2019.

[18] Ling, X., Wang, H., Huang, S., Xia, F. & Dresselhaus, M. S. The renaissance of black phosphorus. Proceedings of the National Academy of Sciences 112, 4523–4530 (**2015**).

[19] Lin, S., Li, Y., Qian, J. & Lau, S. P. Emerging opportunities for black phosphorus in energy applications. Materials Today Energy 12, 1–25 (2019).

[20] Qiu, M. et al. Omnipotent phosphorene: a next-generation, two-dimensional nanoplatform for multidisciplinary biomedical applications. Chemical Society Reviews 47, 5588–5601 (**2018**).

[21] Chen, L. et al. Multifunctional mesoporous black phosphorus-based nanosheet for enhanced tumor-targeted combined therapy with biodegradation-mediated metastasis inhibition. Biomaterials 236, 119770 (**2020**).

[22] Liu, Y. et al. Azide Passivation of Black Phosphorus Nanosheets: Covalent Functionalization Affords Ambient Stability Enhancement. Angewandte Chemie International Edition 58, 1479–1483 (**2019**).

[23] Bridgman, P. W. Two new modifications of phosphorus. Journal of the American Chemical Society 36, 1344–1363 (**1914**).

[24] Shao, J. et al. Biodegradable black phosphorus-based nanospheres for in vivo photothermal cancer therapy. Nature Communications 7 (**2016**).

[25] Pan, W. et al. PRP-chitosan thermoresponsive hydrogel combined with black phosphorus nanosheets as injectable biomaterial for biotherapy and phototherapy treatment of rheumatoid arthritis. Biomaterials 239, 119851 (**2020**).

[26] Sun, Z. et al. New solvent-stabilized few-layer black phosphorus for antibacterial applications. Nanoscale 10, 12543–12553 (**2018**).

[27] Brent, J. R. et al. Production of few-layer phosphorene by liquid exfoliation of black phosphorus. Chem. Commun. 50, 13338–13341 (**2014**).

[28] Lin, S., Chui, Y., Li, Y. & Lau, S. P. Liquid-phase exfoliation of black phosphorus and its applications. FlatChem 2, 15–37 (**2017**).

[29] Cai, W. et al. Natural antioxidant functionalization for fabricating ambient-stable black phosphorus nanosheets toward enhancing flame retardancy and toxic gases suppression of polyurethane. Journal of Hazardous Materials 387, 121971 (**2020**).

[30] Favron, A. et al. Photooxidation and quantum confinement effects in exfoliated black phosphorus. Nature Materials 14, 826–832 (**2015**).

[31] Abate, Y. et al. Recent Progress on Stability and Passivation of Black Phosphorus. Advanced Materials 30, 1704749 (**2018**).

[32] Pei, J. et al. Producing air-stable monolayers of phosphorene and their defect engineering. Nature Communications 7 (**2016**).

[33] Chen, X. et al. High-quality sandwiched black phosphorus heterostructure and its quantum oscillations. Nature Communications 6 (**2015**).

[34] Zhao, Y. et al. Surface Coordination of Black Phosphorus for Robust Air and Water Stability. Angewandte Chemie International Edition 55, 5003–5007 (**2016**).

[35] Ryder, C. R. et al. Covalent functionalization and passivation of exfoliated black phosphorus via aryl diazonium chemistry. Nature Chemistry 8, 597–602 (**2016**).

[36] Mohammadifar, E. et al. Green Synthesis of Hyperbranched Polyglycerol at Room Temperature. ACS Macro Letters 6, 35–40 (**2017**).

[37] Knop, K., Hoogenboom, R., Fischer, D. & Schubert, U. S. Poly(ethylene glycol) in Drug Delivery: Pros and Cons as Well as Potential Alternatives. Angewandte Chemie International Edition 49, 6288–6308 (**2010**).

[38] Abbina, S. et al. Hyperbranched polyglycerols: recent advances in synthesis, biocompatibility and biomedical applications. Journal of Materials Chemistry B 5, 9249–9277 (**2017**).

[39] Deng, Y. et al. The effect of hyperbranched polyglycerol coatings on drug delivery using degradable polymer nanoparticles. Biomaterials 35, 6595–6602 (**2014**).

[40] Mohammadifar, E. et al. One-pot and gram-scale synthesis of biodegradable polyglycerols under ambient conditions: nanocarriers for intradermal drug delivery. Polymer Chemistry 8, 7375–7383 (**2017**).

[41] Hamilton, J. L. et al. In vivo efficacy, toxicity and biodistribution of ultralong circulating desferrioxamine based polymeric iron chelator. Biomaterials 102, 58–71 (**2016**).

[42] Singhvi, M. S., Zinjarde, S. S. & Gokhale, D. V. Polylactic acid: synthesis and biomedical applications. Journal of Applied Microbiology 127, 1612–1626 (**2019**).

[43] Singhvi, M. & Gokhale, D. Biomass to biodegradable polymer (PLA). RSC Advances 3, 13558 (**2013**).

[44] Zabihi, F. et al. Synthesis of poly(lactide-co-glycerol) as a biodegradable and biocompatible polymer with high loading capacity for dermal drug delivery. Nanoscale 10, 16848–16856 (**2018**).

[45] Becker, G. & Wurm, F. R. Functional biodegradable polymers via ring-opening polymerization of monomers without protective groups. Chemical Society Reviews 47, 7739–7782 (**2018**).

[46] Elsawy, M. A., Kim, K.-H., Park, J.-W. & Deep, A. Hydrolytic degradation of polylactic acid (PLA) and its composites. Renewable and Sustainable Energy Reviews 79, 1346–1352 (**2017**).

[47] Hajighasemi, M. et al. Biochemical and Structural Insights into Enzymatic Depolymerization of Polylactic Acid and Other Polyesters by Microbial Carboxylesterases. Biomacromolecules 17, 2027–2039 (**2016**).

[48] Choi, J. R. et al. Black Phosphorus and its Biomedical Applications. Theranostics 8, 1005–1026 (**2018**).

[49] Luo, M., Fan, T., Zhou, Y., Zhang, H. & Mei, L. 2D Black Phosphorus–Based Biomedical Applications. Advanced Functional Materials 29, 1808306 (**2019**).

[50] Shirata, C. et al. Near-infrared photothermal/photodynamic therapy with indocyanine green induces apoptosis of hepatocellular carcinoma cells through oxidative stress. Scientific Reports 7 (**2017**).

[51] Sun, Z. et al. Ultrasmall Black Phosphorus Quantum Dots: Synthesis and Use as Photothermal Agents. Angewandte Chemie International Edition 54, 11526–11530 (**2015**).

[52] Wang, J. et al. Cationic amphiphilic drugs self-assemble to the core–shell interface of PEGylated phospholipid micelles and stabilize micellar structure. Philosophical Transactions of the Royal Society A: Mathematical, Physical and Engineering Sciences 371, 20120309 (**2013**).

[53] Tao, W. et al. Black Phosphorus Nanosheets as a Robust Delivery Platform for Cancer Theranostics. Advanced Materials 29, 1603276 (**2017**).

[54] Wang, H. et al. Ultrathin Black Phosphorus Nanosheets for Efficient Singlet Oxygen Generation. Journal of the American Chemical Society 137, 11376–11382 (**2015**).

[55] Song, S.-J. et al. Comparison of cytotoxicity of black phosphorus nanosheets in different types of fibroblasts. Biomaterials Research 23 (**2019**).

[56] Wang, J. et al. PEGylated-folic acid–modified black phosphorus quantum dots as near-infrared agents for dual-modality imaging-guided selective cancer cell destruction. Nanophotonics 0 (**2020**).

Appendix - Supplementary data

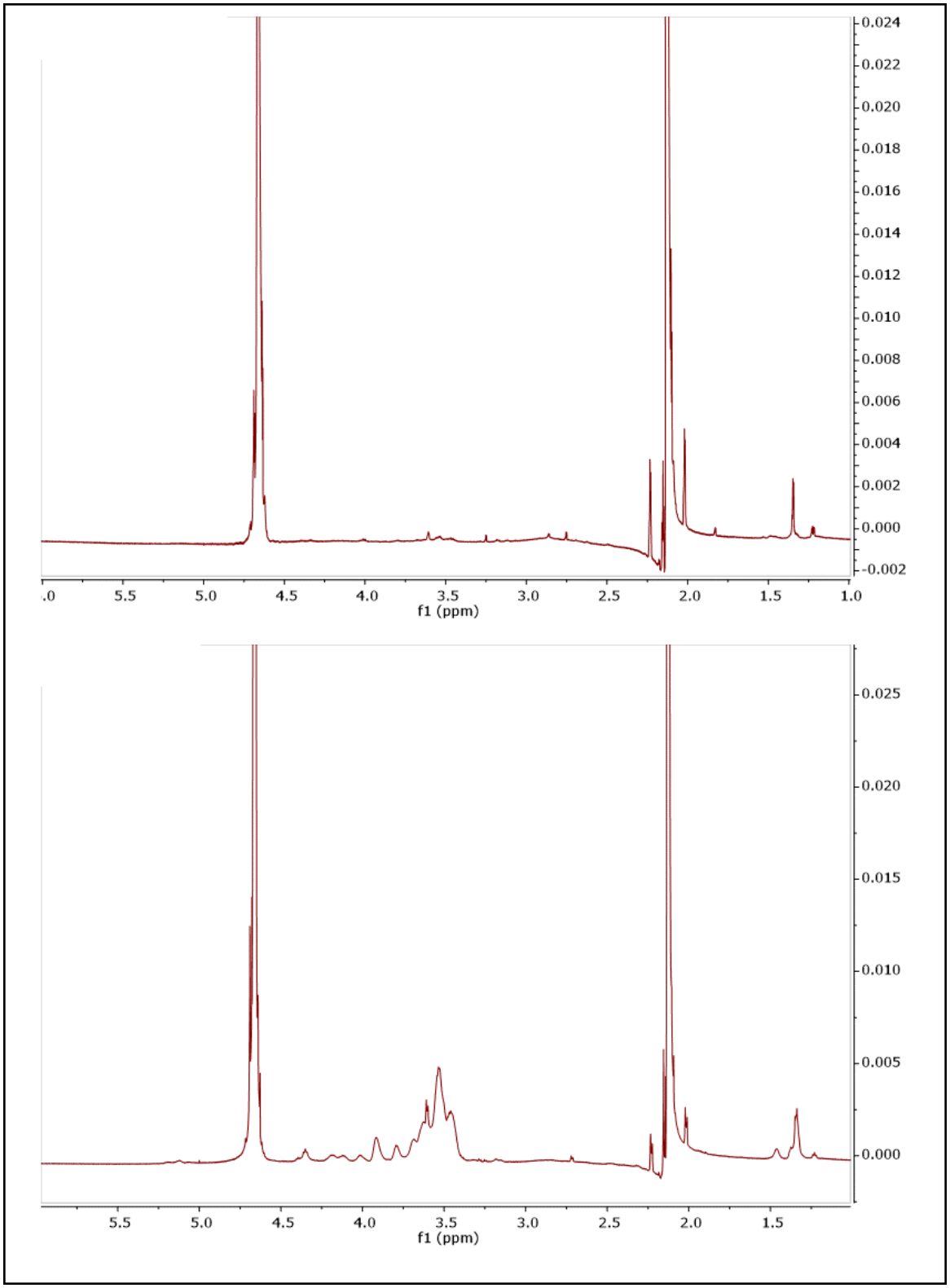

Figure 21 – ^{1}H-NMR of BP-PLA-PG (1:1) (top) and BP-PLA-PG (1:2) (bottom) measured in D_2O.

Universität Basel

Philosophisch-Naturwissenschaftliche Fakultät

Erklärung zur wissenschaftlichen Redlichkeit
(beinhaltet Erklärung zu Plagiat und Betrug)

Bachelorarbeit / Masterarbeit *(nicht Zutreffendes bitte streichen)*

Titel der Arbeit *(Druckschrift)*:

Biological Characterization of Functionalized Black Phosphorus Nanosheets

Name, Vorname *(Druckschrift)*: Wichmann, Natalie

Matrikelnummer: 15-059-330

Hiermit erkläre ich, dass mir bei der Abfassung dieser Arbeit nur die darin angegebene Hilfe zuteil wurde und dass ich sie nur mit den in der Arbeit angegebenen Hilfsmitteln verfasst habe.

Ich habe sämtliche verwendeten Quellen erwähnt und gemäss anerkannten wissenschaftlichen Regeln zitiert.

Diese Erklärung wird ergänzt durch eine separat abgeschlossene Vereinbarung bezüglich der Veröffentlichung oder öffentlichen Zugänglichkeit dieser Arbeit.

☐ ja ☒ nein

Ort, Datum: Steinen, 25.02.20

Unterschrift: N. Wichmann

Dieses Blatt ist in die Bachelor-, resp. Masterarbeit einzufügen.

Januar 2017